

Signs of Non-Monotonic Finite-Volume Corrections to g_A

Zack Hall,^{1,2} Dimitra A. Pefkou,^{3,2} Aaron S. Meyer,⁴ Thomas R. Richardson,^{3,2} Raúl A. Briceño,^{3,2}
M.A. Clark,⁵ Martin Hoferichter,⁶ Emanuele Mereghetti,⁷ Henry Monge-Camacho,⁸
Colin Morningstar,⁹ Amy Nicholson,¹ Pavlos Vranas,^{4,2} and André Walker-Loud^{2,3,4}

¹*Department of Physics and Astronomy, University of North Carolina, Chapel Hill, NC 27516-3255, USA*

²*Nuclear Science Division, Lawrence Berkeley National Laboratory, Berkeley, CA 94720, USA*

³*Department of Physics, University of California, Berkeley, CA 94720, USA*

⁴*Lawrence Livermore National Laboratory, Livermore, CA 94550, USA*

⁵*NVIDIA Corporation, 2701 San Tomas Expressway, Santa Clara, CA 95050, USA*

⁶*Albert Einstein Center for Fundamental Physics, Institute for Theoretical Physics, University of Bern, Sidlerstrasse 5, 3012 Bern, Switzerland*

⁷*Theoretical Division, Los Alamos National Laboratory, Los Alamos, NM 87545, USA*

⁸*National Center For Computational Sciences Oak Ridge National Laboratory, Oak Ridge, Tennessee, USA*

⁹*Department of Physics, Carnegie Mellon University, Pittsburgh, Pennsylvania 15213, USA*

We study finite-volume (FV) corrections to determinations of g_A via lattice quantum chromodynamics (QCD) using analytic results and numerical analysis. We observe that $SU(2)$ Heavy Baryon Chiral Perturbation Theory does not provide an unambiguous prediction for the sign of the FV correction, which is not surprising when one also considers large- N_c constraints on the axial couplings. We further show that non-monotonic FV corrections are naturally allowed when one considers either including explicit Δ -resonance degrees of freedom or one works to higher orders in the chiral expansion. We investigate the potential impact of these FV corrections with a precision study of g_A using models of FV corrections that are monotonic and non-monotonic. Using lattice QCD data that is approximately at the 1% level of precision, we do not see significant evidence of non-monotonic corrections. Looking forward to the next phase of lattice QCD calculations, we estimate that calculations that are between the 0.1%–1%-level of precision may be sensitive to these FV artifacts. Finally, we present an update of the CalLat prediction of g_A in the isospin limit with sub-percent precision, $g_A^{\text{QCD}} = 1.2674(96)$.

I. INTRODUCTION

The nucleon axial coupling, g_A , is a critical quantity for determining many nuclear physics processes, from the primordial abundances of hydrogen and helium formed during Big Bang Nucleosynthesis [1], to our theoretical understanding of Solar Fusion [2], and to relating precision measurements of nuclear β decay rates to Standard Model (SM) parameters [3]. Measurements of g_A from the β -asymmetry of ultracold neutron decays have yielded an experimental value at the 0.1% precision level, but with some tension between the results [4–13] that go into the PDG average [14]. The most precise measurement has a total uncertainty of 0.04% [11].

There is currently a $\sim 4\sigma$ discrepancy between beam [15–18] and bottle [19–27] measurements of the neutron lifetime (τ_n), which depends upon g_A , inspiring suggestions of a light dark-matter particle [28]. However, a recent beam measurement at J-PARC [29] has been found to be consistent with the bottle measurements. Ref. [30] points out that the bottle measurements are consistent with recent measurements of g_A . A theoretical prediction of g_A with a 0.2% precision could discriminate between the two lifetime measurements with the same precision as the beam measurements, using the relation [31, 32],

$$\tau_n(1 + 3\lambda^2)|V_{ud}|^2 = 4902.3(1.3) \text{ s}, \quad (1.1)$$

where $\lambda = g_A/g_V$ and V_{ud} is the Cabibbo-Kobayashi-Maskawa (CKM) matrix element.

However, the value of g_A in this formula, and as reported by experiments and in the PDG, contains radiative QED corrections. While many of these corrections are accounted for [3, 33–40], it has recently been pointed out that there are previously unrealized structure-dependent QED corrections to g_A that may be as large as 2% [41]. This amount is estimated with $SU(2)$ Heavy Baryon Chiral Perturbation Theory (HB χ PT) [42, 43], and thus dependent upon unknown low-energy constants (LECs). This means that presently lattice QCD (LQCD) calculations of g_A [44–50], which are performed in the isospin limit, cannot be directly compared to the experimental determination within the current percent-level of LQCD precision. Refs. [51, 52] propose strategies, such as LQCD+QED calculations that can be used to determine these QED corrections, and thus determine the unknown LECs.

The importance of obtaining sub-percent theoretical predictions for g_A is further exemplified in the context of precision tests of the first row of the CKM matrix. In the SM, $\Delta_{\text{CKM}} = |V_{ud}|^2 + |V_{us}|^2 + |V_{ub}|^2 - 1 = 0$, yet there currently exists a 3σ deficit from unitarity [53] which could be due to beyond-the-SM (BSM) physics. Precision measurements of τ_n and g_A are critical to render the determination of $|V_{ud}|$ from neutron decay competitive with superallowed β decays [54–56]. While the aforemen-

tioned QED corrections to g_A do not impact the determination of $|V_{ud}|$, since they cancel in Eq. (1.1), comparison of LQCD predictions of g_A to the experimental measurements places competitive constraints on BSM right-handed charged currents (RHCCs) [57]. A recent study considering high-energy collider observables, low-energy charged-current processes, and electroweak precision observables has shown that, within an SM effective field theory (EFT) framework, scenarios including RHCCs are most preferred for explaining this unitarity tension [58]. At present, LQCD calculations of g_A allow one to test RHCCs at the level of $\epsilon_R = -0.2(1.2) \times 10^{-2}$ [41, 45, 46] (using the normalization of Ref. [59]), while the unitarity deficit points to $\epsilon_R = -0.69(27) \times 10^{-3}$ [53], strongly motivating further improvements.

Originally, g_A served as an important benchmark quantity to demonstrate that LQCD could precisely reproduce important, known experimental results of relevance to nuclear physics [60]. In recent years, it has become a key quantity for precision tests of the SM and for testing our low-energy understanding of QCD through stringent constraints on LECs of HB χ PT [61].

Motivated by a desire for sub-percent precision results for g_A , we explore the effects of the FV on LQCD calculations of this quantity and examine the behavior of the results as a function of volume (L^3) and pion mass (m_π). For sufficiently large volumes, $m_\pi L \gg 1$, artifacts due to the volume are exponentially suppressed, $\mathcal{O}(e^{-m_\pi L})$ [62]. As a result, one might naïvely expect these systematic effects to be simple to parameterize and monotonically vanish as $L \rightarrow \infty$. However, prior to more recent results, there was a systematic deficit in LQCD results for g_A as compared with the PDG value which became more discrepant as m_π was reduced towards the physical pion mass. This led to speculation that g_A had particularly large FV corrections [63] (which was refuted in Ref. [64]) which may be the source of this discrepancy [65] and that $m_\pi L > 6$ may be required to keep FV corrections $\lesssim 1\%$ [66]. It is now understood that this discrepancy arose from uncontrolled excited state contamination [44, 45, 67].

Because the precision of LQCD calculations of g_A has increased, we scrutinize FV effects as they become more relevant as statistical uncertainties decrease. In particular, we note that the sign of the approach to infinite volume (IV) at heavy pion mass differs with the expectation from HB χ PT suggesting that these effects might be *non-monotonic* with respect to variations m_π and/or $m_\pi L$. With this context in mind, our main goal is to understand the potential shortcomings of previous treatments of FV that have ignored potential non-monotonic FV effects and to present a new strategy to arrive at a final uncertainty that accounts for this FV systematic. We investigate the pion mass dependence of such FV trends and explore the sensitivity of a final quoted result for g_A to the use of various IV extrapolation formulae, including those predicted by HB χ PT. We take the opportunity to update the CalLat prediction from Refs. [45, 68].

II. THEORETICAL EXPECTATIONS AND NUMERICAL OBSERVATIONS

A. Numerical observations of FV corrections

In Ref. [45], CalLat observed the central values of g_A trending upwards with decreasing volume at $m_\pi \approx 220$ MeV, consistent with the leading FV prediction from $SU(2)$ HB χ PT without explicit Δ degrees of freedom (HB χ PT(Δ)) [69], though the trend was not statistically significant (see the upper panel of Fig. 1). The previously unpublished data at $m_\pi \simeq 310$ MeV plotted in the middle panel of Fig. 1 shows the opposite trend with mild statistical significance. In both cases, the precision of these results is also compatible with no FV dependence at the $\sim 1\sigma$ level. All CalLat data used in this study is tabulated in Table II. RQCD has computed g_A at several volumes (and lattice spacings in the range $a \simeq 0.064 - 0.086$ fm) for $m_\pi \simeq 285$ MeV, showing a statistically significant trend that the FV corrections to g_A are negative at this pion mass [48]. This is seen on the bottom panel of Fig. 1, while the plotted RQCD results are listed in Table I.

B. Expectations from χ PT and large N_c

From an EFT perspective, it is not surprising that the FV corrections to g_A are more complex than for other quantities, particularly in comparison with meson quantities. First, the chiral expansion for nucleon quantities is a series in ϵ_π , defined as

$$\epsilon_\pi \equiv \frac{m_\pi}{\Lambda_\chi}, \quad \Lambda_\chi \equiv 4\pi F_\pi, \quad (2.1)$$

where F_π is the pion decay constant. For pions, the expansion is in powers of ϵ_π^2 and so higher-order chiral corrections are relatively more important for nucleons.

Second, several resonances are strongly coupled to the nucleon and of relatively low mass excitation. In particular, the mass gap to the Δ -resonance at the physical point is small, $\Delta \equiv m_\Delta - m_N \simeq 293$ MeV, and decreases as the pion mass increases [70]. The Δ -resonances are also strongly coupled to the nucleon, both through QCD dynamics as well as through large electroweak couplings that govern $N \rightarrow \Delta$ matrix elements. Therefore, the Δ s make significant contributions to many quantities, adding another channel of important radiative virtual corrections [43, 71–75].

Third, for g_A , as for other quantities, the large- N_c expansion places constraints on radiative corrections. These constraints do not need to be imposed, but emerge naturally from the Feynman rules in $SU(2)$ HB χ PT with Δ degrees of freedom (HB χ PT(Δ)). This theory has an additional small parameter to control the perturbative expansion and is sometimes referred to as the small-scale

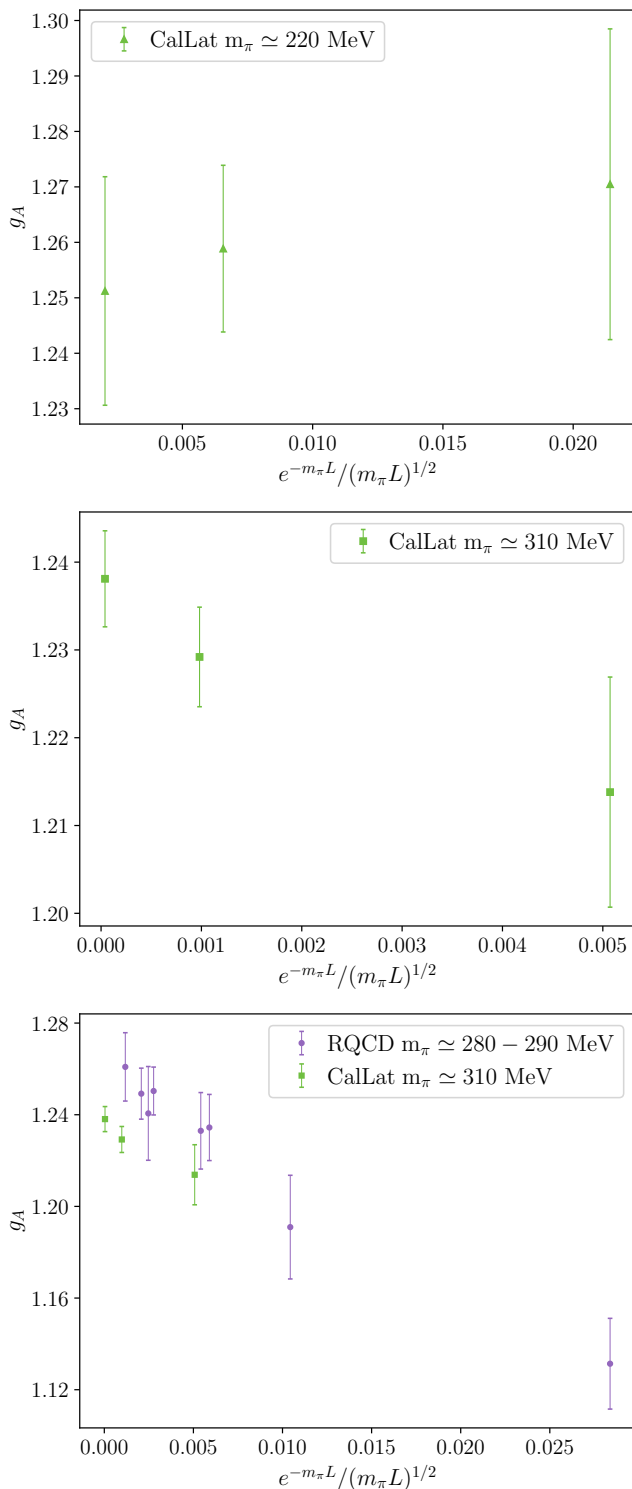


FIG. 1. Top: We plot the results from Ref. [45] for $m_\pi \simeq 220$ MeV and $a \simeq 0.12$ fm. Middle: The data point at the smallest volume with $m_\pi \simeq 310$ MeV and $a \simeq 0.12$ fm from Ref. [45], with two new ensembles at larger volumes analyzed for this work. Bottom: The volume dependence of data published by RQCD [48] at $m_\pi \simeq (280-290)$ MeV.

expansion [76],

$$\epsilon_\Delta = \frac{\Delta}{\Lambda_\chi}. \quad (2.2)$$

For g_A , there are significant cancellations between contributions with virtual Δ -resonance states and those with virtual nucleon states [43]. These cancellations are evident with the use of phenomenological values of the LECs and become manifest when the large- N_c expansion is used to relate them [71, 73, 77–79]. These cancellations also hold for the FV corrections, as we will now discuss.

In $SU(2)$ HB χ PT(Δ), the expression for g_A at next-to-leading order (NLO) in the chiral expansion is [69, 80]¹

$$\begin{aligned} g_A^{(\Delta)} = & g_0 [1 - \epsilon_\pi^2 \ln \epsilon_\pi^2] + \epsilon_\pi^2 (4\tilde{d}_{16}^{r,\Delta} - g_0^3) \\ & - 2\epsilon_\pi^2 \ln \epsilon_\pi^2 \left[g_0^3 + \frac{1}{9} g_0 g_{N\Delta}^2 + \frac{25}{81} g_\Delta g_{N\Delta}^2 \right] \\ & - R \left(\frac{m_\pi^2}{\Delta^2} \right) g_{N\Delta}^2 \left[\epsilon_\pi^2 \frac{32}{27} g_0 + \epsilon_\Delta^2 \left(\frac{76}{27} g_0 + \frac{100}{81} g_\Delta \right) \right] \\ & + \frac{32}{27} g_0 g_{N\Delta}^2 \epsilon_\pi^2 \left[1 + \ln \frac{4\epsilon_\Delta^2}{\epsilon_\pi^2} + \frac{\pi \epsilon_\pi}{\epsilon_\Delta} \right] \\ & + \frac{2}{81} g_{N\Delta}^2 \epsilon_\pi^2 (9g_0 + 25g_\Delta) [1 + \ln(4\epsilon_\Delta^2)], \quad (2.3) \end{aligned}$$

where the non-analytic function is

$$R(z) = \begin{cases} \sqrt{1-z} \ln \left(\frac{1-\sqrt{1-z}}{1+\sqrt{1-z}} \right) + \ln(4/z), & z \leq 1 \\ 2\sqrt{z-1} \arctan(z) + \ln(4/z), & z > 1 \end{cases}, \quad (2.4)$$

and we have defined $\tilde{d}_{16}^{r,\Delta} = (4\pi F)^2 d_{16}^{r,\Delta}$. Each of the axial couplings, g_0 , $g_{N\Delta}$, and g_Δ , represent the leading-order (LO) contribution to the axial charges of the nucleon, the nucleon-to- Δ transition, and Δ , respectively. As such, they all scale like N_c [77, 84, 85]. Because g_A scales like N_c , and the radiative corrections scale like $g^3/F^2 \sim N_c^2$ ($F^2 \sim N_c$) with $g \in \{g_0, g_\Delta, g_{N\Delta}\}$, all corrections with three powers of these axial couplings must exactly cancel in the large- N_c limit.

One can consider the large- N_c expansion about $N_c \rightarrow \infty$ or about large but finite N_c , which leads to two different relations at LO in the large- N_c expansion between the axial couplings [86]:

$$\begin{aligned} N_c = \infty : & \quad \Delta = 0, \quad g_{N\Delta} = \frac{3}{2} g_0, \quad g_\Delta = -\frac{9}{5} g_0, \quad (2.5) \\ N_c \neq \infty : & \quad \Delta = 0, \quad g_{N\Delta} = \frac{6}{5} g_0, \quad g_\Delta = -\frac{9}{5} g_0, \quad (2.6) \end{aligned}$$

¹ This expression is derived in App. A from that given in Ref. [69]. $d_{16}^{r,\Delta}$ is defined in such a way that for $\Delta \rightarrow \infty$ it coincides with d_{16}^r in the conventions of Ref. [81–83]. The Δ parameters are related to those of Ref. [75] by $g_{N\Delta} = \sqrt{2} h_A$ and $g_\Delta = -g_1$.

Both the former [75, 77, 78, 84, 87] and the latter [73, 79, 85, 88–91] commonly appear in the literature. The difference between these two is formally $\mathcal{O}(N_c^{-2})$. Using the expansion about $N_c \rightarrow \infty$, Eq. (2.5), the cancellation between all terms that scale as g_0^3 is explicit. This can be verified by inserting these relations into Eq. (2.3), yielding the result

$$\lim_{N_c \rightarrow \infty} g_A^{(\Delta)} = g_0 + \epsilon_\pi^2 \left[-g_0 \ln \epsilon_\pi^2 + 4\tilde{d}_{16}^{\tilde{r}, \Delta} \right]. \quad (2.7)$$

This expression is contrasted with that in $SU(2)$ HB χ PT(Δ) at same order in ϵ_π ,

$$g_A^{(\Delta)} = g_0 + \epsilon_\pi^2 \left[-g_0(1 + 2g_0^2) \ln \epsilon_\pi^2 + 4\tilde{d}_{16}^{\tilde{r}} - g_0^3 \right]. \quad (2.8)$$

As $g_0 \simeq 1.2$, the coefficient of the $\epsilon_\pi^2 \ln \epsilon_\pi^2$ term in HB χ PT(Δ) is much larger than one would expect starting from HB χ PT(Δ). That LQCD results for g_A show

such mild pion mass dependence is evidence that the large- N_c expansion provides at least a good qualitative guide for understanding chiral corrections to g_A as it naturally reduces the size of corrections at a given order through the large- N_c -predicted opposite-sign contributions from virtual Δ corrections [43, 80].

Similar constraints hold when considering FV corrections, which at NLO are given by $\delta_{\text{FV}}^{(2)} + \delta_{\text{FV}}^{(2, \Delta)}$ [69], where

$$\delta_{\text{FV}}^{(2)} = g_0 \frac{8}{3} \epsilon_\pi^2 \left[g_0^2 F_1^{(2)}(m_\pi L) + F_3^{(2)}(m_\pi L) \right], \quad (2.9)$$

$$\delta_{\text{FV}}^{(2, \Delta)} = g_0 \frac{8}{3} \epsilon_\pi^2 \left[g_{N\Delta}^2 \left(1 + \frac{25}{81} \frac{g_\Delta}{g_0} \right) F_2^{(2)}(m_\pi L, \Delta L) + g_{N\Delta}^2 F_4^{(2)}(m_\pi L, \Delta L) \right], \quad (2.10)$$

and the FV functions $F_i^{(2)}$ are defined in Ref. [69],

$$\begin{aligned} F_1^{(2)}(x) &= \sum_{\vec{n} \neq 0} \left[K_0(x|\vec{n}|) - \frac{K_1(x|\vec{n}|)}{x|\vec{n}|} \right], & F_3^{(2)}(x) &= -\frac{3}{2} \sum_{\vec{n} \neq 0} \frac{K_1(x|\vec{n}|)}{x|\vec{n}|}, \\ F_2^{(2)}(x, y) &= -\sum_{\vec{n} \neq 0} \left[\frac{K_1(x|\vec{n}|)}{x|\vec{n}|} + \frac{y^2 - x^2}{x^2} K_0(x|\vec{n}|) - \frac{y}{x^2} \int_x^\infty dz \frac{2zK_0(z|\vec{n}|) + (y^2 - x^2)|\vec{n}|K_1(z|\vec{n}|)}{\sqrt{z^2 + y^2 - x^2}} \right], \\ F_4^{(2)}(x, y) &= \frac{8}{9} \sum_{\vec{n} \neq 0} \left[\frac{K_1(x|\vec{n}|)}{x|\vec{n}|} - \frac{\pi e^{-x|\vec{n}|}}{2y|\vec{n}|} - \frac{y^2 - x^2}{x^2 y} \int_x^\infty dz \frac{zK_0(z|\vec{n}|)}{\sqrt{z^2 + y^2 - x^2}} \right]. \end{aligned} \quad (2.11)$$

$K_n(x)$ are modified Bessel functions of the second kind. As with the IV corrections, a careful implementation of the large- N_c limit at fixed quark mass, Eq. (2.5), leads to an exact cancellation of all corrections that scale like g_0^3 . In this limit, one would predict that the leading FV correction to g_A is given by

$$\delta_{\text{FV}}^{(2)} + \delta_{\text{FV}}^{(2, \Delta)} \rightarrow -4\epsilon_\pi^2 g_0 \sum_{\vec{n} \neq 0} \frac{K_1(m_\pi L|\vec{n}|)}{m_\pi L|\vec{n}|}. \quad (2.12)$$

In contrast, the leading FV correction in HB χ PT(Δ) is

$$\begin{aligned} \delta_{\text{FV}}^{(2)} &= 4\epsilon_\pi^2 g_0 \sum_{\vec{n} \neq 0} \left[\frac{2}{3} g_0^2 K_0(m_\pi L|\vec{n}|) \right. \\ &\quad \left. - \left(1 + \frac{2}{3} g_0^2 \right) \frac{K_1(m_\pi L|\vec{n}|)}{m_\pi L|\vec{n}|} \right]. \end{aligned} \quad (2.13)$$

For values of $m_\pi L \gtrsim 3$ and $g_0 \simeq 1.2$, the first term is larger than the second term and so the predicted FV correction is positive, while the leading prediction from HB χ PT(Δ) after application of the large- N_c expansion is negative for any value of $m_\pi L$.

The full NLO prediction for the HB χ PT(Δ) FV correction will lie somewhere between these limits. We estimate them as follows. First, we plot the predicted FV

correction from HB χ PT(Δ) as a function of ϵ_π while setting $m_\pi L = 4$ and $g_0 = 1.20(05)$, see Fig. 2. Next, we set $\Delta = 293$ MeV and then approximate $g_{N\Delta}$ and g_Δ according to Eq. (2.5) while adding an extra uncertainty from the large N_c expansion, e.g. $g_{N\Delta} = \frac{3}{2}(g_0 + (0, 1/N_c^2))$. We plot the same correction except using the finite N_c relation $g_{N\Delta} = \frac{6}{5}(g_0 + (0, 1/N_c^2))$, Eq. (2.6) and, finally, the prediction with Eq. (2.5) and $\Delta = 0$. The spread of these predictions demonstrates that our present knowledge is insufficient to predict the sign of the NLO FV correction without further input. It would be ideal to have LQCD calculations of the $N \rightarrow \Delta$ axial transition matrix elements and the Δ axial charge [92, 93], which could be used to make more precise predictions for these FV corrections, to be compared with more precise LQCD results of g_A at different volumes and pion masses. To this end, we note that also the full next-to-next-to-leading-order (N²LO) results including Δ degrees of freedom and FV corrections are available, see App. B for the complete expressions.

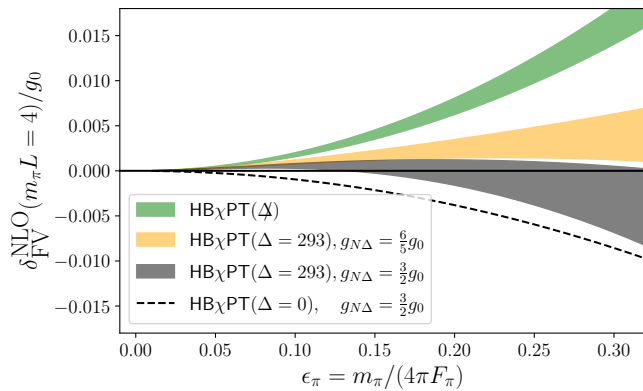


FIG. 2. We plot the predicted NLO FV corrections to g_A using $SU(2)$ $\text{HB}\chi\text{PT}(\Delta)$ and the large- N_c expansion, with two different large- N_c relations for $g_{N\Delta}$. We also plot the predicted FV correction from $\text{HB}\chi\text{PT}(\Delta)$ and the large- N_c expansion also with $\Delta = 0$. All corrections are plotted with $m_\pi L = 4$.

III. QUANTIFYING THE FV UNCERTAINTY

When accounting for FV corrections to g_A , the strategy used by most groups is to use the asymptotic form of the leading prediction from $SU(2)$ $\text{HB}\chi\text{PT}(\Delta)$

$$\delta_{\text{FV}} = c_V m_\pi^2 \frac{e^{-m_\pi L}}{\sqrt{m_\pi L}}, \quad (3.1)$$

which can be obtained from Eq. (2.13) by expanding the Bessel functions for large argument and replacing the coefficient predicted by $\text{HB}\chi\text{PT}(\Delta)$ with c_V . This parameter is then determined by fitting results at heavier than physical pion mass, typically in a global analysis simultaneously with discretization corrections as well as quark mass dependence [44, 46, 48, 49]. Under the assumption that the FV corrections are non-monotonic versus pion mass, an important question to resolve is at what level of precision will the above model introduce an error?

In order to estimate the potential impact of the FV model, we perform the following exercise: first, we pick a specific model to describe the pion mass dependence and two models of the FV corrections, one that is monotonic and one that supports non-monotonicity. In order to create this model, we use $SU(2)$ $\text{HB}\chi\text{PT}(\Delta)$ at N²LO, for which g_A is given by

$$g_A = g_0 + \delta_\chi^{(2)} + \delta_\chi^{(3)} + \delta_{\text{FV}}^{(2)} + \delta_{\text{FV}}^{(3)}, \quad (3.2)$$

where the superscript, n , denotes the order in ϵ_π^n at which a term contributes (see also App. B for a summary of all corrections). The IV chiral corrections are given by [81]

$$\begin{aligned} \delta_\chi^{(2)} &= \epsilon_\pi^2 \left[-g_0(1 + 2g_0^2) \ln \epsilon_\pi^2 + 4\tilde{d}_{16}^r - g_0^3 \right], \\ \delta_\chi^{(3)} &= \epsilon_\pi^3 g_0 \frac{2\pi}{3} \left[3(1 + g_0^2) \frac{4\pi F}{M_0} + 4(2\tilde{c}_4 - \tilde{c}_3) \right], \end{aligned} \quad (3.3)$$

where the LECs are defined as

$$F = \lim_{m_\pi \rightarrow 0} F_\pi, \quad \tilde{c}_i = (4\pi F)c_i, \quad \tilde{d}_i^r = (4\pi F)^2 d_i^r, \quad (3.4)$$

such that \tilde{c}_i and \tilde{d}_i^r are dimensionless. Note that the use of ϵ_π in these expressions, rather than $m_\pi/(4\pi F)$, induces higher-order corrections beginning at $\mathcal{O}(\epsilon_\pi^4)$, which should be accounted for if the next-to-next-to-next-to-leading (N³LO) expression is used to fit g_A results (see Refs. [45, 94]).

The NLO FV corrections are given in Eq. (2.9), while the N²LO ones are

$$\begin{aligned} \delta_{\text{FV}}^{(3)} &= \epsilon_\pi^3 g_0 \frac{2\pi}{3} \left\{ g_0^2 \frac{4\pi F}{M_0} F_1^{(3)}(m_\pi L) \right. \\ &\quad \left. - \left[\frac{4\pi F}{M_0} (3 + 2g_0^2) + 4(2\tilde{c}_4 - \tilde{c}_3) \right] F_3^{(3)}(m_\pi L) \right\}, \end{aligned} \quad (3.5)$$

with

$$\begin{aligned} F_1^{(3)}(x) &= \sum_{\vec{n} \neq \vec{0}} \frac{K_{\frac{1}{2}}(x|\vec{n}|)}{\sqrt{\frac{\pi}{2}x|\vec{n}|}} x|\vec{n}| = \sum_{\vec{n} \neq \vec{0}} e^{-x|\vec{n}|}, \\ F_3^{(3)}(x) &= \sum_{\vec{n} \neq \vec{0}} \frac{K_{\frac{3}{2}}(x|\vec{n}|)}{\sqrt{\frac{\pi}{2}x|\vec{n}|}} = \sum_{\vec{n} \neq \vec{0}} \frac{e^{-x|\vec{n}|}}{x|\vec{n}|}. \end{aligned} \quad (3.6)$$

With these functional pieces defined, we proceed to study the potential impact of different choices in modeling the FV corrections.

A. FV sensitivity study: a cautionary tale

To study the impact of the FV model used, we undertake the following exercise:

1. We begin by fitting the CalLat results at lattice spacing $a \simeq 0.12$ fm listed in Table II to the IV expression,

$$g_A = g_0 + \delta_\chi^{(2)} + \delta_\chi^{(3)}, \quad (3.7)$$

utilizing only the largest volume at a given pion mass. We use this fit to provide an estimate for the LECs

$$g_0^{\text{FV}}, \quad \tilde{c}_{34}^{\text{FV}} = 2\tilde{c}_4^{\text{FV}} - \tilde{c}_3^{\text{FV}}, \quad (3.8)$$

that we will use to estimate the FV corrections. In $\delta_\chi^{(3)}$, we set $M_0 = 939$ MeV and $F = 92.3$ MeV as the difference using these values and their respective chiral-limit values is higher order in the chiral expansion. We focus on a single lattice spacing to isolate the FV effects.

2. We use the RQCD results [48] at $m_\pi \simeq (280\text{--}290)$ MeV, listed in Table I and shown in the bottom panel of Fig. 1, to construct two models of FV corrections:

- (a) Monotonic FV model: Using the value of g_0^{FV} from step one, we fit the RQCD data to the model

$$g_A^{285} = g_0^{285} + f_2 \delta_{\text{FV}}^{(2)}(g_0^{\text{FV}}), \quad (3.9)$$

where f_2 is priored as a Gaussian distribution of zero mean and width of $\sigma = 1$.

- (b) Non-monotonic FV model: Using the values of g_0^{FV} and $\tilde{c}_{34}^{\text{FV}}$ from step 1, as well as the same values of M_0 and F , we fit the RQCD data to the model

$$g_A^{285} = g_0^{285} + \delta_{\text{FV}}^{(2)}(g_0^{\text{FV}}) + f_3 \delta_{\text{FV}}^{(3)}(g_0^{\text{FV}}, \tilde{c}_{34}^{\text{FV}}), \quad (3.10)$$

where f_3 is priored as a Gaussian distribution of zero mean and width of $\sigma = 1$.

3. We then fit the full $a \simeq 0.12$ fm data set listed in Table II with two models

$$g_A^{\text{mono}} = g_0 + \delta_{\chi}^{(2)}(g_0^{\text{IV}}) + \delta_{\chi}^{(3)}(g_0^{\text{IV}}, \tilde{c}_{34}^{\text{IV}}) + f_2 \delta_{\text{FV}}^{(2)}(g_0^{\text{FV}}), \quad (3.11a)$$

$$g_A^{\text{non-mono}} = g_0 + \delta_{\chi}^{(2)}(g_0^{\text{IV}}) + \delta_{\chi}^{(3)}(g_0^{\text{IV}}, \tilde{c}_{34}^{\text{IV}}) + \delta_{\text{FV}}^{(2)}(g_0^{\text{FV}}) + f_3 \delta_{\text{FV}}^{(3)}(g_0^{\text{FV}}, \tilde{c}_{34}^{\text{FV}}), \quad (3.11b)$$

where the LECs in the IV and FV functions are kept separate, with the FV values determined in step 1 used in the FV functions and the values of f_2 or f_3 taken from step 2. The resulting analysis is used to predict g_A at the physical pion mass for which we find

$$\begin{aligned} g_A^{(3.11a)} &= 1.284(12), \\ g_A^{(3.11b)} &= 1.266(12), \end{aligned} \quad (3.12)$$

showing tension between these models for the final prediction even at the $\mathcal{O}(1\%)$ uncertainty level.

4. We repeat step 3, while artificially decreasing the statistical uncertainty on the $a \simeq 0.12$ fm data by a common rescaling factor and compare the prediction from these two models as a function of the final total uncertainty on the predicted value of g_A at the physical pion mass and IV. The results from this study are plotted in Fig. 3.

This exercise demonstrates that the choice of FV model can have a statistically significant systematic impact on the predicted final value of g_A . For results at the percent level and more precise, it is important to incorporate a set of models with sufficient flexibility to support non-monotonic FV corrections and compare the extrapolation with monotonic FV models. Otherwise, one may invariably introduce an unquantified systematic uncertainty that is comparable to, or larger than, the statistical uncertainty.

This particular study was performed under the assumption that the RQCD results could be used to determine the coefficients of the FV model. A more realistic study would add these models in a global analysis,

TABLE I. Data from Ref. [48] shown in Fig. 1c, and used in the FV study of Sec. III A. We also estimate the value of ϵ_π for each CLS ensemble by scaling ϵ_π on our a12m310XL ensemble with the ratio of pion masses where we convert our pion mass to MeV units using the scale setting in Ref. [95]: $\epsilon_\pi = \epsilon_\pi^{\text{a12m310XL}} \times (m_\pi/m_\pi^{\text{a12m310XL}})$.

Ensemble	m_π [MeV]	ϵ_π	$m_\pi L$	a [fm]	g_A
N101	281	0.2216	5.86	0.086	1.261(15)
N451	289	0.2279	5.34	0.076	1.249(11)
N401	287	0.2263	5.30	0.076	1.241(20)
N450	287	0.2263	5.30	0.076	1.250(10)
N201	287	0.2263	4.49	0.064	1.234(14)
N200	286	0.2255	4.47	0.064	1.233(17)
H105	281	0.2216	3.91	0.086	1.191(23)
S201	290	0.2287	3.02	0.064	1.131(20)

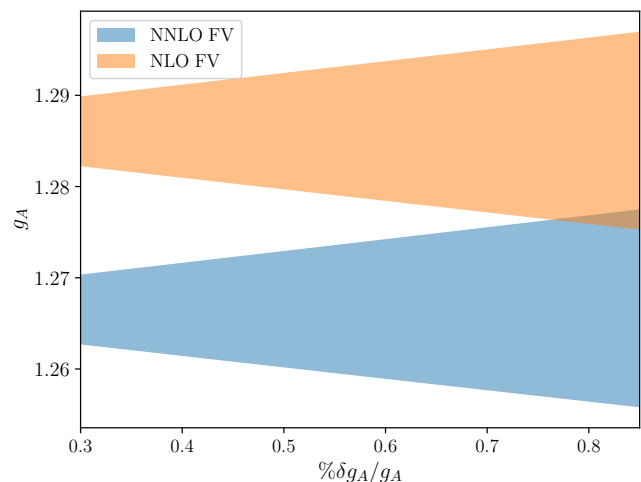


FIG. 3. Using the strategy outlined in the FV study, we plot the value of g_A , as function of the relative percent uncertainty, $\delta g_A/g_A$. The top band is determined by utilizing Eq. (3.11a) with NLO FV corrections, while the bottom band includes corrections up to N²LO, Eq. (3.11b).

including discretization effects. One challenge in isolating the FV corrections to g_A is that they are comparable in size to the observed discretization effects. In principle, these corrections should be independent through the separation of short- and long-distance scales of the problem. In practice, because the FV corrections are assessed by fitting coefficients multiplying FV correction terms, their contributions become entangled with discretization corrections through the analysis procedure and the two effects can influence each other, including changing the sign of the leading FV or discretization corrections depending upon the model for these systematic effects.

IV. UPDATED g_A RESULT WITH MDWF/HISQ

We update the results in Ref. [45], which utilized a mixed lattice action [96, 97] with $N_f = 2 + 1 + 1$ Highly Improved Staggered Quarks (HISQ) [98] in the sea and Möbius Domain Wall Fermion (MDWF) [99, 100] quarks in the valence sector. The gauge links were smoothed with gradient flow [101, 102] prior to using them in the Dirac operator, resulting in our MDWF/HISQ action [103]. Some of the HISQ ensembles were generated by the MILC Collaboration [104, 105], while the rest were generated by the CalLat Collaboration [45, 95, 106] including a new ensemble first used in this work.

Table II lists the resulting values of g_A , ϵ_π , $m_\pi L$, and a/w_0 on each ensemble needed for the extrapolation analysis, where w_0 is the gradient flow scale defined in Ref. [109]. The short-hand naming key [110] indicates the approximate lattice spacing and pion mass on the given ensemble, with a12m130 indicating a lattice spacing of $a \simeq 0.12$ fm and a pion mass of $m_\pi \simeq 130$ MeV, for example. For details of the input parameters of the action, see Refs. [95, 103, 106]. The analysis of the correlation functions is described in Ref. [45]: a constant is fit to the m_{res} correlation function and multi-state fits are performed to the pion correlation function to determine m_π and F_π on each ensemble; the values of \mathring{g}_A and \mathring{g}_V , which give $g_A = (Z_A/Z_V)(\mathring{g}_A/\mathring{g}_V)$, with $Z_A/Z_V - 1 \lesssim 1 \times 10^{-4}$ [45], are determined with a multi-state fit to the nucleon two-point correlation function and the ‘‘Feynman-Hellmann’’ correlation functions described in Ref. [111]. Further details of the correlator analysis will be provided in a forthcoming publication.

The results in the upper part of the table are from Ref. [45]. The results on the a12m310L and a12m310XL ensemble are new to this work and enable a volume study at $m_\pi \simeq 310$ MeV in addition to that possible with the a12m220 set of ensembles. The results on the a12m130 and a15m135XL ensembles were first reported in Ref. [68]. For a12m130, we changed the quark smearing from that in Ref. [45] to that in Ref. [106] and increased the number of sources per configuration from 3 to 32. The result a15m135XL is obtained from a newly generated ensemble and uses 8 sources per configuration on 1000 configurations.

A. Models considered

In this updated g_A calculation, we use both quantitative and qualitative models of the FV corrections that are allowed to be non-monotonic as predicted from χ PT, as well as more agnostic non- χ PT inspired monotonic models. These are studied in conjunction both with χ PT expressions for the IV corrections as well as simple Taylor expansion expressions. For the χ PT models, we only consider the expressions from $SU(2)$ HB χ PT(Δ). This

is because our numerical results are not sufficient to constrain the new parameters describing the axial $N \rightarrow \Delta$ transitions or the axial coupling of the Δ , and we wish to minimize the influence from phenomenological input. For the quantitative χ PT model, we use the expressions given in Eqs. (2.9) and (3.5).

The quark-mass dependence of g_A is parameterized using four models,

$$g_{A,\chi} = g_0 + \delta_\chi^{(2)} + \delta_\chi^{(3)}, \quad (4.1a)$$

$$g_{A,\text{pol}}^{(1)} = c_0 + c_1 \epsilon_\pi + c_2 \epsilon_\pi^2, \quad (4.1b)$$

$$g_{A,\text{pol}}^{(2)} = c_0 + c_2 \epsilon_\pi^2 + c_3 \epsilon_\pi^3, \quad (4.1c)$$

$$g_{A,\text{pol}}^{(3)} = c_0 + c_2 \epsilon_\pi^2 + c_4 \epsilon_\pi^4. \quad (4.1d)$$

In the above we include the HB χ PT(Δ) prediction together with simple Taylor expansions in different powers of ϵ_π^n , as was done in Refs. [45, 68]. We keep the total number of parameters c_i fixed across the polynomial models. Equation (4.1c) was not used in the previous work. This model can be considered as HB χ PT(Δ) with the chiral logarithms set to zero.

Meanwhile, the non-monotonic FV corrections models used are

$$g_{A,\text{FV}} = \delta_{\text{FV}}^{(2)} + \delta_{\text{FV}}^{(3)}, \quad (4.2a)$$

$$g_{A,\text{FV}}^{f_2} = f_2 \delta_{\text{FV}}^{(2)} + \delta_{\text{FV}}^{(3)}, \quad (4.2b)$$

$$g_{A,\text{FV}}^{f_3} = \delta_{\text{FV}}^{(2)} + f_3 \delta_{\text{FV}}^{(3)}, \quad (4.2c)$$

$$g_{A,\text{FV}}^{f_2, f_3} = f_2 \delta_{\text{FV}}^{(2)} + f_3 \delta_{\text{FV}}^{(3)}. \quad (4.2d)$$

The above models use the full N²LO expressions for the FV corrections, and in the case of the later three include different choices of unknown coefficients f_2 and f_3 . The purpose of these latter three models is to use χ PT to guide the analytic form of the IV corrections, but allow for the strength of the FV corrections to become decoupled from the values of the LECs needed to describe the IV pion mass dependence of model $g_{A,\chi}$. We augment this set with four additional χ PT-agnostic models

$$g_{A,\text{FV}}^{\text{mon-1}} = f_2 \epsilon_\pi^2 F_1^{(2)}, \quad (4.3a)$$

$$g_{A,\text{FV}}^{\text{mon-2}} = f_2 \epsilon_\pi^2 F_3^{(2)}, \quad (4.3b)$$

$$g_{A,\text{FV}}^{\text{mon-3}} = f_2 \epsilon_\pi^2 F_1^{(3)}, \quad (4.3c)$$

$$g_{A,\text{FV}}^{\text{mon-4}} = f_2 \epsilon_\pi^2 F_3^{(3)}, \quad (4.3d)$$

which are all monotonic by construction, and have their $m_\pi L$ dependence parameterized by the FV functions defined in Eqs. (2.11) and (3.6). The purpose of these additional models is to diagnose whether statistically significant evidence of the non-monotonic behavior predicted by χ PT, which we observed as a trend in the $a \simeq 0.12$ fm data and the RQCD data in the previous section, can be detected in a global analysis of our full dataset.

Finally, the discretization effects are parameterized up to $\mathcal{O}(a^4)$ in the Symanzik expansion [112, 113]. For

TABLE II. Results of ϵ_π , $m_\pi L$, a/w_0 , and g_A on each ensemble used in this work. The results in the top part of the table are from Ref. [45] and the four ensembles in the bottom are updated (a12m130) or new. The ensembles generated by CalLat used the MILC code with the a12m310L, a12m310XL, and a15m135XL ones also using QUDA [107, 108]. We also list the source (first publication) where each ensemble was used.

Ensemble	Source	ϵ_π	$m_\pi L$	a/w_0	g_A
a15m400	Ref. [45]	0.30374(54)	4.8	0.9201(12)	1.2154(60)
a12m400	Ref. [45]	0.29840(52)	5.8	0.73335(43)	1.2162(97)
a09m400	Ref. [45]	0.29819(54)	5.8	0.53516(77)	1.2097(80)
a15m350	Ref. [45]	0.27412(52)	4.2	0.9101(11)	1.197(14)
a12m350	Ref. [45]	0.27063(69)	5.1	0.72701(58)	1.235(14)
a09m350	Ref. [45]	0.26949(58)	5.1	0.52910(73)	1.227(15)
a15m310	Ref. [104]	0.24957(36)	3.8	0.90261(73)	1.215(12)
a12m310	Ref. [104]	0.24486(51)	4.5	0.72134(62)	1.214(13)
a09m310	Ref. [104]	0.24619(44)	4.5	0.52449(61)	1.235(11)
a15m220	Ref. [105]	0.18084(31)	4.0	0.88849(63)	1.274(14)
a12m220	Ref. [105]	0.18220(44)	4.3	0.70942(55)	1.259(15)
a12m220L	Ref. [105]	0.18155(42)	5.4	0.70972(35)	1.251(21)
a12m220S	Ref. [105]	0.18418(57)	3.3	0.71078(81)	1.270(28)
a09m220	Ref. [105]	0.18197(37)	4.7	0.51578(32)	1.2519(85)
a12m310L	This work	0.24295(40)	6.0	0.72084(46)	1.2292(57)
a12m310XL	Ref. [95]	0.24318(39)	9.0	0.72124(31)	1.2381(55)
a12m130	Ref. [105]	0.11343(32)	3.9	0.70368(30)	1.266(13)
a15m135XL	Ref. [106]	0.11486(20)	4.9	0.88347(31)	1.273(13)

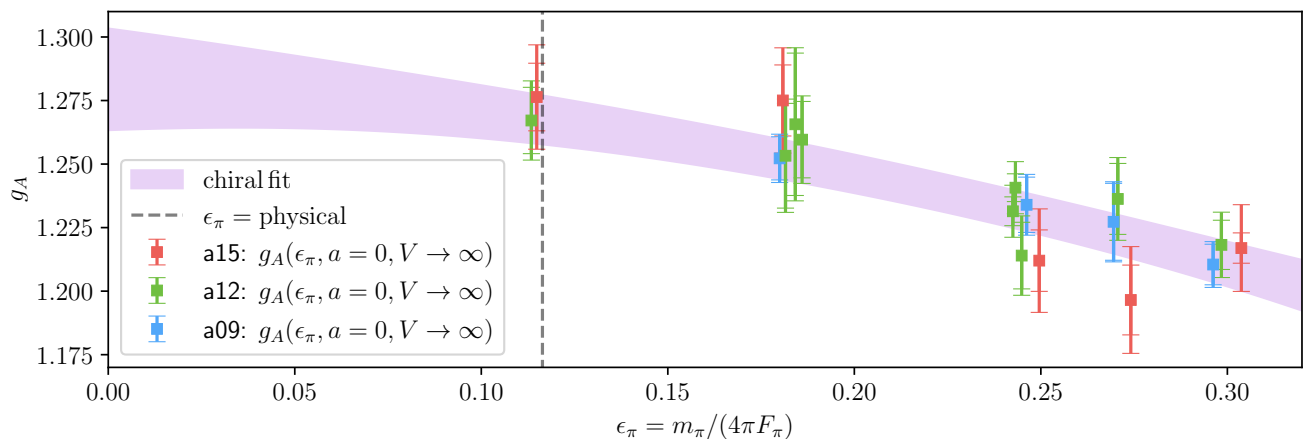


FIG. 4. Our final fit for the pion mass dependence of g_A model-averaged over all 64 models considered, as described in Sec. IV A, plotted along the values of g_A extrapolated to the continuum and IV limits. The outer error bars correspond to the uncertainty of the extrapolated results, while the inner ones to the uncertainties of the original values listed in Table II. Some of the data has been slightly shifted in the x -axis for visibility.

this mixed action with valence fermions that respect chiral symmetry, the leading discretization effects begin at $\mathcal{O}(a^2)$ [114]. We parameterize them as

$$g_{A,a}^{(2)} = a_2 \epsilon_a^2, \quad (4.4a)$$

$$g_{A,a}^{(4)} = a_2 \epsilon_a^2 + b_4 \epsilon_a^2 \epsilon_\pi^2 + a_4 \epsilon_a^4, \quad (4.4b)$$

with

$$\epsilon_a^2 = \frac{a^2}{4w_0^2}. \quad (4.5)$$

The values for ϵ_a for the ensembles used besides a12m310L were previously determined in Ref. [95].

We consider these two models for the discretization dependence together with all combinations of the pion mass and FV dependence listed above, resulting in 64 different models. We fit the parameters of each model by χ^2 minimization using the `lsqfit` package, and include a discussion on the choice of Bayesian priors in App. C. We use the posterior distributions to interpolate to the physical point. We take the FLAG definition of the isospin symmetric point [115]

$$m_\pi^{\text{iso,phys}} = 135 \text{ MeV},$$

$$F_\pi^{\text{iso,phys}} = \frac{130.5}{\sqrt{2}} = 92.3 \text{ MeV},$$

$$\epsilon_{\pi}^{\text{iso,phys}} = 0.1164. \quad (4.6)$$

The resulting central values and errors for g_A are model-averaged weighted by the Bayes factors of the corresponding model fit as was done previously [45, 68].

B. Final results and comparison with other works

The final result we obtain for $g_A = 1.2674(96)$, with a percentage uncertainty of 0.76%,

$$\begin{aligned} g_A &= 1.2674(79)^{\text{s}}(28)^{\chi}(05)^{\text{FV}}(38)^{\text{a}}(26)^{\text{M}} \\ &= 1.2674(96). \end{aligned} \quad (4.7)$$

The uncertainty breakdown into the statistical (s), chiral extrapolation (χ), FV, and discretization (a) is done by differentiating the final posterior prediction at the physical point with respect to the relevant priors. The statistical uncertainty is with respect to the g_A data and ϵ_{π} , while the FV uncertainty arises from the f_2 and f_3 coefficients when relevant, for example. The final model-selection uncertainty arises from the variance of the models with respect to the Bayes Model Average value, see Refs. [45, 106] for further details.

The model-averaged chiral fit to g_A is plotted in the continuum and IV limits as a function of ϵ_{π} in Fig. 4, along with the individual ensemble values extrapolated to the continuum and to IV. The individual model results including the priors and posteriors for all parameters along with the corresponding Bayes factors are listed in Tables IV and V of App. D.

In Fig. 5, we plot the updated g_A and compare it against other LQCD calculations. On the lower part of the plot, we include the latest FLAG [115] averages which, just like all LQCD results, correspond to QCD-only predictions. In Ref. [41], it was estimated that pion-induced radiative corrections to g_A are

$$g_A^{\text{PDG}} = g_A^{\text{QCD}}(1 + \delta_{\text{RC}}), \quad \delta_{\text{RC}} = 2.0(6) \times 10^{-2}. \quad (4.8)$$

We propagate these estimates to the FLAG $N_f = 2 + 1$ and $N_f = 2 + 1 + 1$ predictions, and plot the resulting values, denoted as FLAG + QED † , on the bottom of the plot, just above the PDG value $g_A = 1.2754(13)$ [14].

At our current LQCD precision, the FV dependence of our data is small and modeling these corrections contributes the least to the final uncertainty. The result of a global analysis using just the χ PT and χ PT-inspired non-monotonic models of Eq. (4.2) is $g_A^{\text{non-mon}} = 1.2672(96)$, which is consistent with the value $g_A^{\text{mon}} = 1.2674(96)$ obtained by the monotonic FV models of Eq. (4.3).

C. $SU(2)$ HB χ PT(Δ) extrapolations

It is interesting to examine the $SU(2)$ HB χ PT(Δ) extrapolations in more detail. This is both because this

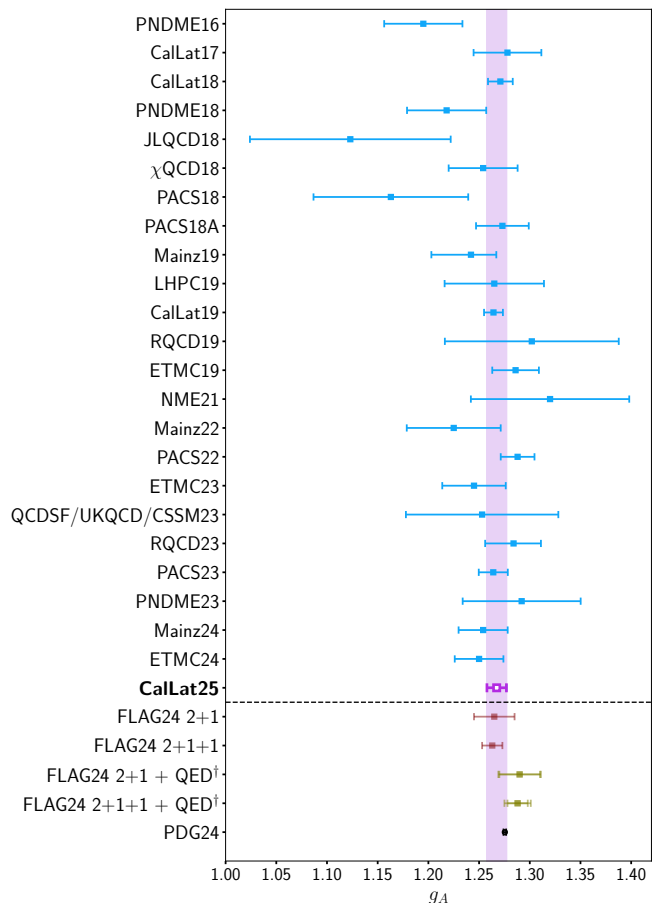


FIG. 5. Comparison of our final value for g_A against several LQCD collaborations [44–50, 68, 116–130], the FLAG average [115], the FLAG average modified to include an estimate of the QED corrections [41], and the PDG average [14].

theory serves as a foundation for many modern applications of chiral EFT to predicting the spectrum and properties of nuclei, see Ref. [131] for a recent review. It also enables us to more stringently test our low-energy understanding of nuclear physics by examining the convergence properties of the theory as well as comparing the LECs determined from comparisons with LQCD versus experimental data.

The first interesting observation is that the $SU(2)$ HB χ PT(Δ) extrapolations have the lowest likelihood of any of the extrapolation models, as can be seen from the logGBF values in Table V. In fact, the strict $SU(2)$ HB χ PT(Δ) model without the f_2 or f_3 FV coefficients (those using Eq. (4.1a) for m_{π} dependence and Eq. (4.2a) for FV corrections) is the least favored of all fits. At the same time, it should be noted that the final extrapolated value is perfectly consistent with all other models. What likely drives these fits to have a lower likelihood than the Taylor expansion fits is that the $\epsilon_{\pi}^2 \ln \epsilon_{\pi}^2$ have large coefficients, and thus the counterterm contributions and higher-order corrections must cancel against each other in order to produce such a mild pion mass dependence.

This is contrasted with the Taylor models which all have $\mathcal{O}(1)$ or smaller coefficients in the expansion, and thus provide a rapidly converging expansion to describe the numerical results. It will be interesting to see if an extrapolation with explicit Δ s, that exhibits milder pion mass dependence, is more favored. Such an extrapolation with only LQCD input will require calculations of $N \rightarrow \Delta$ and $\Delta \rightarrow \Delta$ axial matrix elements. See Ref. [93] for promising first steps in this direction.

The second interesting observation concerns the combination of LECs $2c_4 - c_3$ that appears in Eq. (3.2). A recent phenomenological determination from N³LO analysis of pion–nucleon (πN) scattering data [132, 133] found the following values for the LECs c_3 and c_4 ²

$$\begin{aligned} c_3 &= -5.61(6) \text{ GeV}^{-1}, \\ c_4 &= 4.26(4) \text{ GeV}^{-1}, \\ 2c_4 - c_3 &= 14.1(1) \text{ GeV}^{-1}. \end{aligned} \quad (4.9)$$

In our analysis using Eq. (4.1a) to describe the pion mass dependence of g_A , we utilized the dimensionless versions of these LECs, Eq. (3.4). From Table V, one sees that the posterior values of \tilde{c}_{34} for the $SU(2)$ HB χ PT(Δ) fit models range from 0.76 to 0.81. Converting to GeV^{-1} using $F_\pi = 92.3 \text{ MeV}$, the value of $2c_4 - c_3$ determined from this analysis becomes

$$2c_4 - c_3 = (0.66\text{--}0.70) \text{ GeV}^{-1}, \quad (4.10)$$

which is 20 times smaller than the phenomenological estimate above. The small priors given to \tilde{c}_{34} are not the source of this discrepancy. These values were chosen to optimize the Bayes factor of the fits. If instead a prior width of 50 is used, the posterior value of $\tilde{c}_{34} = 0.85(25)$ or similar is found.

This discrepancy for the LECs observed here is a particularly extreme case, but similar effects have been encountered in other examples, including the determination from πN scattering in the first place [75, 132, 133]. That is, the large values of c_3 and c_4 entering at subleading loop level generate sizable corrections that can differ from case to case, and therefore do not necessarily drop out when comparing observables. In the πN case, this implies that the HB χ PT(Δ) theory is not even accurate enough to relate consistently the expansion of the amplitude around subthreshold and threshold kinematics. The situation improves appreciably when the Δ resonance is included as an explicit degree of freedom [75], as the large loop corrections are reduced, but, for reasons currently not understood, also when resumming higher orders in

the $1/M_0$ expansion into a covariant formulation. Understanding this convergence behavior is important, as the LECs are used extensively to predict two-body nuclear currents and three-body nuclear forces [134–136], see, e.g., Ref. [137] for a discussion how to account for c_i chiral uncertainties in the axial current. The present work suggests that g_A is another quantity particularly sensitive to this issue. Future work that includes the Δ resonance as an explicit degree of freedom, and/or employs covariant formulations of baryon χ PT, could thus provide valuable new perspectives. Understanding the convergence of the chiral expansion is also important for the radiative corrections to g_A , which, at NLO, depend on the combination $c_4 - c_3$ [41]. Also in this case, it will be important to extend the calculation to include the Δ resonance and to thoroughly study the convergence.

V. DISCUSSION AND CONCLUSION

A theoretical prediction of g_A with a sub-percent precision can contribute to tests of the SM, as well as put constraints on BSM right-handed currents [57] that offer a possible explanation for the first-row CKM unitarity tension [58]. At this level of precision, systematic uncertainties from FV and discretization corrections must be scrutinized more carefully to ensure they remain as small as or smaller than the statistical precision. LQCD calculations of g_A all have small discretization errors that are currently compatible with a zero slope with respect to powers of the lattice spacing [44–50], while some of them display statistically significant FV corrections. Therefore, in this work, we have investigated FV corrections in greater detail than has been previously explored in the literature.

Our previous results [45] on three volumes at $m_\pi \simeq 220 \text{ MeV}$ showed a trend, albeit not statistically significant, that is consistent with the predicted FV correction from $SU(2)$ HB χ PT(Δ), Eq. (2.9). Subsequently, we generated new results at different volumes at $m_\pi \simeq 310 \text{ MeV}$ which showed the opposite trend. Further, the RQCD results at $m_\pi \simeq 285 \text{ MeV}$ also showed this opposite trend with statistical significance, see Fig. 1, hinting at the possibility of non-monotonic FV corrections. As discussed in Sec. IIB, non-monotonic FV corrections to g_A would not be surprising as there are significant cancellations from radiative corrections to g_A between virtual contributions involving nucleons and Δ -resonance states. These cancellations are predicted from large- N_c considerations and the cancellations also manifest in the predicted FV corrections.

In Sec. IV, we performed a thorough analysis of our results, Table II, using various models for the pion mass dependence and various models for the FV corrections. We report an updated value of g_A , Eq. (4.7), with a 0.78% relative uncertainty. One interesting finding from our analysis using $SU(2)$ HB χ PT(Δ) to describe the

² The counting of chiral orders refers to the non-trivial ones, and since chiral corrections to g_A start at $\mathcal{O}(e_\pi^2)$, the N³LO results from Refs. [132, 133] are consistent with the N²LO corrections to g_A . This distinction matters since the indicated errors, propagated from the πN input, are subleading compared to the differences between determinations at different chiral orders.

pion mass dependence of g_A is that the value of the LEC $2c_4 - c_3$ we determine is an order of magnitude smaller than the state-of-the-art phenomenological determinations [133]. Going forward, it is important to understand this discrepancy as the phenomenological LECs are utilized to make predictions for properties of nuclei through modern applications of chiral EFT [131]. As in similar cases [75], studies including the Δ resonance as an explicit degree of freedom and/or using covariant formulations could shed light on the convergence properties of the chiral expansion in the baryon sector.

In the FV correction, we included models that were monotonic by construction and models that allow for non-monotonic behavior. With our current level of precision, our numerical results cannot distinguish between these two types of FV corrections. In Sec. III A, we studied the potential sensitivity of using monotonic versus non-monotonic FV models under the assumption that the numerical results are sufficiently precise to constrain the FV corrections, finding that as the total uncertainty is reduced below a percent, the FV systematic can become a larger uncertainty than the statistical uncertainty. We conclude that going forward, for sub-percent determinations of g_A , it is important to utilize models of FV corrections that support non-monotonic as well as monotonic behavior, at least if the final result depends upon heavier than physical pion mass results to perform all extrapolations.

As noted in Sec. I, LQCD results for g_A must not be compared to the PDG value at their current quoted precision because of unaccounted for QED corrections, estimated to be 2% using $SU(2)$ HB χ PT(Δ) and phenomenological values of some of the LECs [41]. The estimate relied upon Naïve Dimensional Analysis [138] as one of the LECs has not been constrained. Therefore, to take advantage of the present and future precision of LQCD results of g_A , it is necessary to carry out a determination of these QED corrections with LQCD+QED calculations, as suggested for example in Ref. [51, 52].

ACKNOWLEDGMENTS

We thank Jacobo Ruiz de Elvira for ongoing collaboration on the chiral extrapolation of g_A [139]. The LQCD calculations were carried out on Summit at the Oak Ridge Leadership Computing Facility at the Oak Ridge National Laboratory, which is supported by the Office of Science of the U.S. Department of Energy under Contract No. DE-AC05-00OR22725, through the Innovative and Novel Computational Impact on Theory and Experiment (INCITE) program; on Sierra at Lawrence Livermore National Laboratory (LLNL) through an Early Science Award; and on Lassen at LLNL through the LLNL Computing Grand Challenge Program.

The computations were performed with LALIBE [140] which utilizes the Chroma software suite [141] with QUDA solvers [107, 108] and HDF5 [142] for I/O [143]. The calculations were efficiently managed with METAQ [144, 145]. The HMC was performed with the MILC Code [146], and for the ensembles new in this work, running on GPUs using QUDA. The final extrapolation analysis utilized `gvar` [147] and `lsqfit` [148].

This work was supported by the NVIDIA Corporation (MAC); by the U.S. National Science Foundation (NSF) through the Mathematical and Physical Sciences Ascending Postdoctoral Research Fellowship under award No. 2402482 (ZH), under NSF Award PHY-2209167 (CM), by the NSF through cooperative agreement 2020275 (TRR), and under the NSF Faculty Early Career Development Program (CAREER) under award PHY-2047185 (AN,ZH); by the U.S. Department of Energy (DOE), Office of Science, Office of Nuclear Physics, under grant contract numbers DE-SC0004658 (DAP), No. 89233218CNA000001 (EM), DE-AC52-07NA27344 (ASM, PV), DE-AC02-05CH11231 (ZH, RB, AWL), DE-AC05-00OR22725 (HJM), by the Office of Science Graduate Student Research Program (ZH), the Neutrino Theory Network Program Grant DE-AC02-07CHI11359 and U.S. Department of Energy DE-SC0020250 (ASM), through the “Nuclear Theory for New Physics” Topical Collaboration award No. DE-SC0023663 (TRR, ZH, AWL, EM), and the Swiss National Science Foundation, Project No. TMC2-2.213690 (MH).

Appendix A: NLO χ PT formula for $g_A^{(\Delta)}$

The FV corrections to g_A in $SU(2)$ HB χ PT(Δ) that arise at NLO were derived in Ref. [69]. The IV formulae were also provided and, as written there, given by

$$\begin{aligned} \delta_\chi^{(2)} &= -i \frac{2}{3F^2} \left[\frac{3}{2} g_0 R_1(m_\pi, \mu) + 4g_0^3 J_1(m_\pi, 0, \mu) \right], \\ \delta_\chi^{(2,\Delta)} &= -i \frac{2}{3F^2} \left[4 \left(g_{N\Delta}^2 g_0 + \frac{25}{81} g_{N\Delta}^2 g_\Delta \right) J_1(m_\pi, \Delta, \mu) - \frac{32}{9} g_{N\Delta}^2 g_0 N_1(m_\pi, \Delta, \mu) \right], \end{aligned} \quad (\text{A1})$$

where the non-analytic functions are defined as

$$\begin{aligned}
iR_1(m, \mu) &= \frac{m^2}{(4\pi)^2} \ln \frac{m^2}{\mu^2}, \\
iJ_1(m, \Delta, \mu) &= \frac{3}{4} \frac{\Delta^2}{(4\pi)^2} \left[\left(\frac{m^2}{\Delta^2} - 2 \right) \ln \frac{m^2}{\mu^2} + 2\sqrt{1 - \frac{m^2}{\Delta^2}} \ln \frac{1 - \sqrt{1 - \frac{m^2}{\Delta^2}}}{1 + \sqrt{1 - \frac{m^2}{\Delta^2}}} \right], \\
iN(m, \Delta, \mu) &= \frac{3}{4} \frac{\Delta^2}{(4\pi)^2} \left[\left(\frac{m^2}{\Delta^2} - \frac{2}{3} \right) \ln \frac{m^2}{\mu^2} + \frac{2\pi}{3} \frac{m^3}{\Delta^3} + \frac{2}{3} \left(1 - \frac{m^2}{\Delta^2} \right)^{3/2} \ln \frac{1 - \sqrt{1 - \frac{m^2}{\Delta^2}}}{1 + \sqrt{1 - \frac{m^2}{\Delta^2}}} \right], \tag{A2}
\end{aligned}$$

and one can show the latter two functions have the limit

$$iN_1(m, 0, \mu) = iJ_1(m, 0, \mu) = \frac{3}{4} \frac{m^2}{(4\pi)^2} \ln \frac{m^2}{\mu^2}. \tag{A3}$$

It is convenient to define subtracted functions for the purpose of chiral extrapolations:

$$\bar{J}_1(m, \Delta, \mu) = J_1(m, \Delta, \mu) - J_1(m, 0, \mu), \quad \bar{N}_1(m, \Delta, \mu) = N_1(m, \Delta, \mu) - N_1(m, 0, \mu), \tag{A4}$$

such that the parameter g_0 in the extrapolation functions is $g_0 = \lim_{m_\pi \rightarrow 0} g_A$. This amounts to a renormalization of g_0 in the Lagrangian, which we call \mathring{g}_0 ,

$$g_0 = \mathring{g}_0(\mu) + \frac{4\Delta^2}{(4\pi F)^2} \ln \frac{\Delta^2}{\mu^2} \frac{\mathring{g}_{N\Delta}^2}{81} (57\mathring{g}_0 + 25\mathring{g}_\Delta). \tag{A5}$$

The NLO loop contribution to g_A can then be expressed as

$$\delta_\chi^{(2)} + \delta_\chi^{(2,\Delta)} \Big|_{\text{loop}} = -(g_0 + 2g_0^3) \epsilon_\pi^2 \ln \frac{m_\pi^2}{\mu^2} - \frac{8}{3} \left(g_{N\Delta}^2 g_0 + \frac{25}{81} g_{N\Delta}^2 g_\Delta \right) \frac{i\bar{J}_1(m_\pi, \Delta, \mu)}{\Lambda_\chi^2} + \frac{64}{27} g_0 g_{N\Delta}^2 \frac{i\bar{N}_1(m_\pi, \Delta, \mu)}{\Lambda_\chi^2}, \tag{A6}$$

where

$$\begin{aligned}
\frac{i\bar{J}_1(m_\pi, \Delta, \mu)}{\Lambda_\chi^2} &= \frac{3}{4} \epsilon_\pi^2 \left[\frac{m_\pi^2}{\Delta^2} \ln \frac{m_\pi^2}{\mu^2} + 2R \left(\frac{m_\pi^2}{\Delta^2} \right) \right], \\
\frac{i\bar{N}_1(m_\pi, \Delta, \mu)}{\Lambda_\chi^2} &= \frac{3}{4} \epsilon_\pi^2 \ln \frac{m_\pi^2}{\mu^2} + \frac{\pi}{2} \epsilon_\pi^2 \frac{m_\pi}{\Delta} + \frac{1}{2} \epsilon_\pi^2 \ln \frac{4\Delta^2}{m_\pi^2} + \frac{1}{2} (\epsilon_\Delta^2 - \epsilon_\pi^2) R \left(\frac{m_\pi^2}{\Delta^2} \right), \tag{A7}
\end{aligned}$$

and $R(z)$ is defined in Eq. (2.4). Finally, we redefine $\tilde{d}_{16}^{\tilde{r},\Delta}$ such that the decoupling of the Δ -resonance is explicit in the limit $\Delta \rightarrow \infty$ and so that our definition agrees with Refs. [81–83]. Inserting these into the previous expression and subtracting all corrections proportional to $g_{N\Delta}^2$ in the heavy- Δ limit yields Eq. (2.3).

Appendix B: N²LO FV functions with explicit Δ s

The full N²LO result including Δ degrees of freedom and FV corrections can be expressed as

$$g_A = g_0 + \delta_\chi^{(2)} + \delta_\chi^{(3)} + \delta_{\text{FV}}^{(2)} + \delta_{\text{FV}}^{(3)} + \delta_\chi^{(2,\Delta)} + \delta_\chi^{(3,\Delta)} + \delta_{\text{FV}}^{(2,\Delta)} + \delta_{\text{FV}}^{(3,\Delta)}, \tag{B1}$$

where the terms without “ Δ ” superscript refer to the IV chiral and FV corrections in $SU(2)$ HB χ PT(Δ) as indicated, while the last four terms refer to the additional effects in HB χ PT(Δ). The individual corrections are given by

$$\begin{aligned}
\delta_\chi^{(2)} &= \epsilon_\pi^2 \left[-g_0(1 + 2g_0^2) \ln \epsilon_\pi^2 + 4\tilde{d}_{16}^{\tilde{r}} - g_0^3 \right], \\
\delta_\chi^{(3)} &= \epsilon_\pi^3 g_0 \frac{2\pi}{3} \left[3(1 + g_0^2) \frac{4\pi F}{M_0} + 4(2\tilde{c}_4 - \tilde{c}_3) \right], \\
\delta_{\text{FV}}^{(2)} &= \frac{8}{3} \epsilon_\pi^2 \sum_{\vec{n} \neq \vec{0}} \left[g_0^3 K_0(x_n) - \frac{g_0(3 + 2g_0^2)}{2x_n} K_1(x_n) \right], \quad x_n = m_\pi L |\vec{n}|,
\end{aligned}$$

$$\begin{aligned}
\delta_{\text{FV}}^{(3)} &= -\epsilon_\pi^3 g_0 \frac{2\pi}{3} \sum_{\vec{n} \neq \vec{0}} \left[\frac{4\pi F}{M_0} (3 + g_0^2 (2 - x_n)) + 4(2\tilde{c}_4 - \tilde{c}_3) \right] \frac{e^{-x_n}}{x_n}, \\
\delta_\chi^{(2,\Delta)} &= -2\epsilon_\pi^2 \ln \epsilon_\pi^2 \left[\frac{1}{9} g_0 g_{N\Delta}^2 + \frac{25}{81} g_\Delta g_{N\Delta}^2 \right] - R \left(\frac{m_\pi^2}{\Delta^2} \right) g_{N\Delta}^2 \left[\epsilon_\pi^2 \frac{32}{27} g_0 + \epsilon_\Delta^2 \left(\frac{76}{27} g_0 + \frac{100}{81} g_\Delta \right) \right] \\
&\quad + \frac{32}{27} g_0 g_{N\Delta}^2 \epsilon_\pi^2 \left[1 + \ln \frac{4\epsilon_\Delta^2}{\epsilon_\pi^2} + \frac{\pi \epsilon_\pi}{\epsilon_\Delta} \right] + \frac{2}{81} g_{N\Delta}^2 \epsilon_\pi^2 (9g_0 + 25g_\Delta) \left[1 + \ln(4\epsilon_\Delta^2) \right], \\
\delta_\chi^{(3,\Delta)} &= -\frac{2g_{N\Delta}^2 \epsilon_\Delta}{243} \frac{4\pi F}{M_0} \left[(63g_0 - 25g_\Delta) \epsilon_\pi^2 + 20(9g_0 + 5g_\Delta) \epsilon_\Delta^2 + \frac{36\sqrt{2}}{g_{N\Delta}} \frac{M_0}{4\pi F} (13\tilde{b}_4 + 12\tilde{b}_5) (\epsilon_\Delta^2 - \epsilon_\pi^2) \right] R \left(\frac{m_\pi^2}{\Delta^2} \right) \\
&\quad + \frac{4g_{N\Delta}^2 \epsilon_\pi^2 \epsilon_\Delta}{243} \frac{4\pi F}{M_0} \left[5(9g_0 + 5g_\Delta) + \frac{9\sqrt{2}}{g_{N\Delta}} \frac{M_0}{4\pi F} (13\tilde{b}_4 + 12\tilde{b}_5) \right] \left[1 + \ln \frac{4\epsilon_\Delta^2}{\epsilon_\pi^2} \right], \\
\delta_{\text{FV}}^{(2,\Delta)} &= \sum_{\vec{n} \neq \vec{0}} \left[-\frac{\epsilon_\pi^3}{\epsilon_\Delta} g_0 g_{N\Delta}^2 \frac{32\pi}{27} \frac{e^{-x_n}}{x_n} - \epsilon_\pi^2 g_{N\Delta}^2 \frac{8}{243} (81g_0 + 25g_\Delta) \int_0^\infty d\lambda \lambda \left[3K_0(y_n) - y_n K_1(y_n) \right] \right. \\
&\quad \left. + \frac{\epsilon_\pi^3}{\epsilon_\Delta} g_0 g_{N\Delta}^2 \frac{64}{27} \int_0^\infty d\lambda \beta \left[K_0(y_n) - \frac{1}{y_n} K_1(y_n) \right] \right], \quad y_n = x_n \sqrt{\beta}, \quad \beta = 1 + \lambda^2 + 2\lambda\xi, \quad \xi = \frac{\Delta}{m_\pi}, \\
\delta_{\text{FV}}^{(3,\Delta)} &= \sum_{\vec{n} \neq \vec{0}} \left[\epsilon_\pi^3 g_{N\Delta}^2 (81g_0 + 25g_\Delta) \frac{4}{243} \frac{4\pi F}{M_0} \int_0^\infty d\lambda \lambda \left[2\xi K_0(y_n) - \frac{\lambda y_n}{\beta} (3\beta - 2\xi^2) K_1(y_n) \right. \right. \\
&\quad \left. \left. + \lambda \left(\frac{y_n}{\beta} \right)^2 (\beta^2 - \xi^3 \lambda + \beta \lambda (\lambda + 3\xi)) K_2(y_n) \right] \right. \\
&\quad \left. + \epsilon_\pi^3 g_0 g_{N\Delta}^2 \frac{32}{27} \frac{4\pi F}{M_0} \int_0^\infty d\lambda \left[(\beta - 4\xi\lambda - 3\lambda^2) K_0(y_n) + \left(\frac{2\beta}{y_n} - \frac{y_n(\beta + \xi\lambda)^2}{\beta} \right) K_1(y_n) \right] \right. \\
&\quad \left. - \epsilon_\pi^3 g_{N\Delta} \frac{16\sqrt{2}}{27} (13\tilde{b}_4 + 12\tilde{b}_5) \int_0^\infty d\lambda \beta \left[K_0(y_n) - \frac{1}{y_n} K_1(y_n) \right] \right], \tag{B2}
\end{aligned}$$

with $\tilde{b}_i = (4\pi F)b_i$ and b_i in the conventions of Ref. [75], where large- N_c estimates are derived, leading to $|b_4 \pm b_5| \leq 5 \text{ GeV}^{-1}$. $\delta_{\text{FV}}^{(2)}$ and $\delta_{\text{FV}}^{(2,\Delta)}$ agree with Eq. (2.10), $\delta_\chi^{(2)}$ and $\delta_\chi^{(2,\Delta)}$ combine to Eq. (2.3). The N²LO FV corrections including Δ s were derived in the context of Refs. [149, 150]. For the N²LO IV expressions, see also Refs. [139, 151].

Appendix C: Choice of Bayesian priors in global fits

The global fits for g_A are performed with functional forms consisting of three terms, parameterizing the quark mass, FV, and discretization dependence. We include four possible choices for the quark mass (Eqs. (4.1)), eight for the FV (Eqs. (4.2) and (4.3)), and two for the discretization dependence (Eqs. (4.5)). The large number of parameters for each of the 64 models considered motivates us to follow a Bayesian approach, and to carefully consider the effect of the choice of priors to the fit results. Our procedure for selecting the priors is described below, while the summary of the final model results for g_A , along with the priors, model weights, and posteriors are listed in Appendix D.

Our knowledge about the physical value of g_A motivates us to set the prior of the parameters g_0 and c_0 of Eq. (4.1) to 1.25(10). For the remaining parameters, we set the central values of the priors to 0, and follow the steps below, motivated by the Empirical Bayes Criterion, to choose the corresponding prior widths. We also note that for all parameters, varying our choices of the prior widths by $\mathcal{O}(1)$ factors does not affect our final results for g_A .

- Chiral dependence:** We first isolate the parameters of the mass-dependence models of Eq. (4.1) by considering fits to the $a12$ data only, choosing the largest volume at the pion masses for which ensembles at multiple volumes are available. We vary the prior widths of the pairs of parameters, $(\tilde{d}_{16}^r, \tilde{c}_{34})$ for $g_{A,\chi}$, (c_1, c_2) for $g_{A,\text{pol}}^{(1)}$, (c_2, c_3) for $g_{A,\text{pol}}^{(2)}$, and (c_2, c_4) for $g_{A,\text{pol}}^{(3)}$, and study the resulting Bayes factors. For $g_{A,\chi}$, there is a maximum in the region we explore for $(\Delta \tilde{d}_{16}^r, \Delta \tilde{c}_{34})$. For the three Taylor models, there is a maximum with respect to Δc_2 , while the dependence on the second parameter of each is small and thus we conservatively set the corresponding priors to those chosen for Δc_2 . Our final prior widths choices are well within the regions where the largest Bayes factors are observed, as seen in the plots of Fig. 6, $(\Delta \tilde{d}_{16}^r, \Delta \tilde{c}_{34}) = (5, 1)$, $(\Delta c_1, \Delta c_2) = (0.5, 0.5)$, $(\Delta c_2, \Delta c_3) = (1, 1)$, and $(\Delta c_2, \Delta c_4) = (1, 1)$.

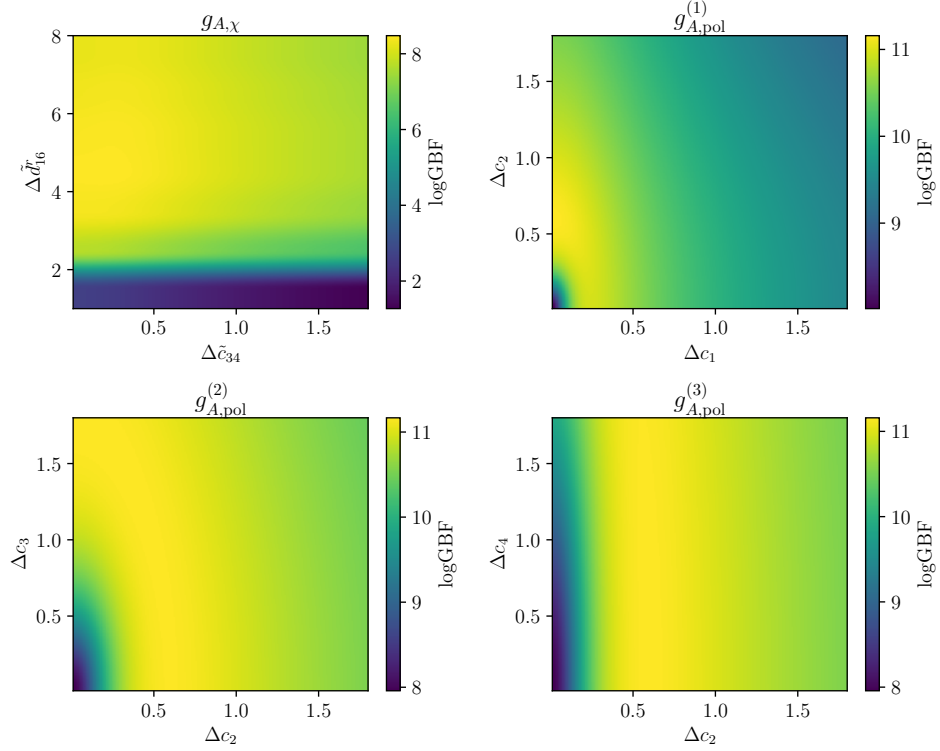


FIG. 6. The log of the Bayes factors obtained by fitting the largest volume a_{12} data using the models of Eqs. (4.1) plotted as functions of the prior width of their free parameters.

- Discretization dependence:** Next, the priors widths for the mass-dependence parameters are frozen and prior widths for parameters with lattice spacing dependence are varied. Our dataset exhibits minimal dependence on the finite lattice spacing, making it impossible to choose optimal prior widths of the parameters a_2 , a_4 , and b_4 defined in Eqs. (4.5) using the Empirical Bayes Criterion. However, we observe that the central value and error of our final model-averaged estimate for g_A is identical for any choice of $\Delta a_2 \gtrsim 0.5$, including those larger by several orders of magnitude. As Δa_2 decreases, the final error becomes smaller and the fit output Bayes factor grows, but simultaneously the probability of the model shrinks by an amount that cannot be quantified. Therefore we choose to set $\Delta a_2 = 0.5$. The dependence of the Bayes factor on the width of the higher-order parameter b_4 is much milder, as seen in on the right side of Fig. 7, therefore we conservatively set the prior $\Delta b_4 = \Delta a_2 = 0.5$. The left side of Fig. 7 shows the dependence of the Bayes factor on the prior width of a_4 and a_2 at fixed b_2 , and it is clear that smaller values of Δa_4 are preferred compared to Δb_4 , so we set its prior to half of Δb_4 , $\Delta a_4 = 0.25$.
- FV dependence:** After having chosen prior widths for the chiral and discretization part of the models as described above, the only parameters that remain are those that are introduced solely by the FV models of Eqs. (4.2) and (4.3), f_2 and f_3 . We again employ the Empirical Bayes Criterion and perform fits to the full dataset using the 48 out of the 64 models that depend on f_2 and/or f_3 , and varying the corresponding prior widths. In this procedure, we set the priors to the remaining parameters, g_0 , \tilde{c}_{34} , \tilde{d}_{16}^r , c_0 , c_1 , c_2 , c_3 , c_4 , a_2 , a_4 , and b_4 to the values described in the previous steps, with the exception of the g_0 that shows up in the FV part of the polynomial models, which is set to 1.2(5) since, in contrast to the χ PT models, it is not tightly constrained by the chiral dependence of the model. Based on the results for the Bayes factor shown in Fig. 8, we choose to set $\Delta f_2 = 1$ for the non-monotonic models, $\Delta f_2 = 2$ for the monotonic models, $\Delta f_3 = 6$ for the $g_{A,\chi} + g_{A,\text{FV}}^{f_3}$ model, and $\Delta f_3 = 1$ for the rest of the models. We only include the results for the discretization model $g_{A,a}^{(2)}$ in the figures, but visually identical results are obtained when using the other discretization model of Eq. (4.5), $g_{A,a}^{(4)}$.

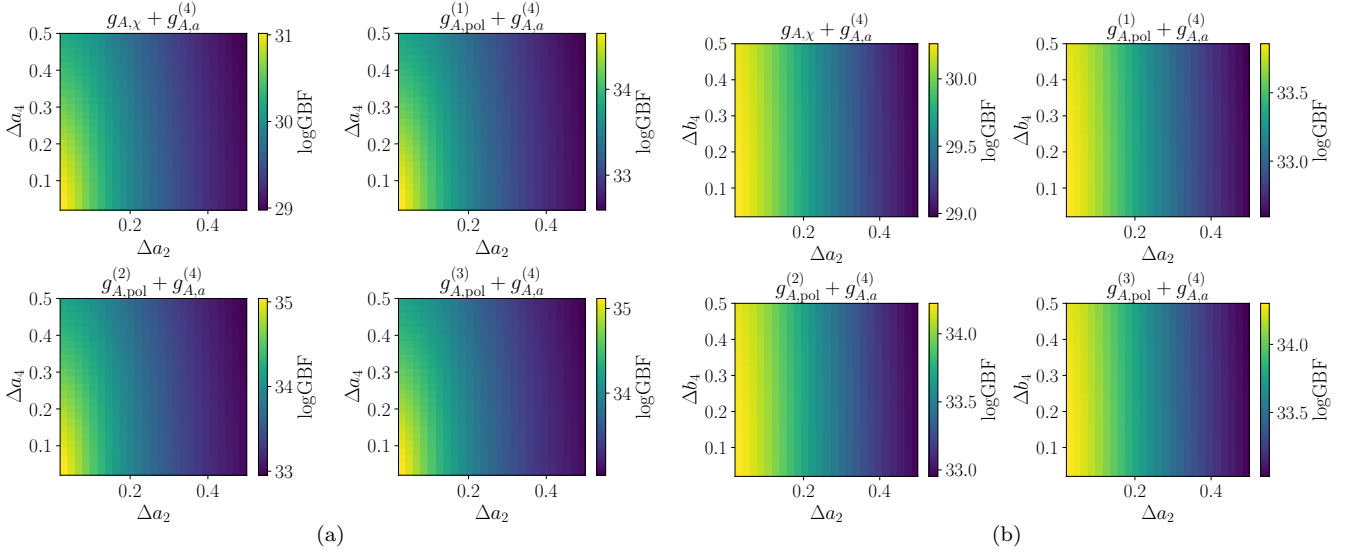


FIG. 7. The log of the Bayes factors obtained by fitting the data at all lattice spacings (keeping the largest volume ensemble for the pion masses for which multiple volumes are available) using the models of Eqs. (4.1) plus the discretization dependence model $g_{A,a}^{(4)}$ defined in Eq. (4.4b). In (a) we fix $\Delta b_4 = 0.5$ and vary a_2 and a_4 , while in (b) we fix $\Delta a_4 = 0.5$ and vary a_2 and b_4 .

Appendix D: Global fit model results

In this appendix, tables are provided summarizing the final choices for fit results. Table III provides the log Gaussian Bayes Factors and model weights along with the posterior distributions for g_A . Table IV provides the list of priors for the fits used in this manuscript. Table V gives the final posterior distributions for the LECs that have been fit in each model.

-
- [1] B. D. Fields, K. A. Olive, T.-H. Yeh, and C. Young, “Big-Bang Nucleosynthesis after Planck,” *JCAP* **03**, 010 (2020), [Erratum: *JCAP* **11**, E02 (2020)], [arXiv:1912.01132 \[astro-ph.CO\]](#).
 - [2] B. Acharya *et al.*, “Solar fusion III: New data and theory for hydrogen-burning stars,” (2024), [arXiv:2405.06470 \[astro-ph.SR\]](#).
 - [3] L. Hayen, “Opportunities and open questions in modern β decay,” *Ann. Rev. Nucl. Part. Sci.* **74**, 497–528 (2024), [arXiv:2403.08485 \[nucl-th\]](#).
 - [4] P. Bopp, D. Dubbers, L. Hornig, E. Klemt, J. Last, H. Schutze, S. J. Freedman, and O. Scharpf, “The Beta Decay Asymmetry of the Neutron and g_A/g_V ,” *Phys. Rev. Lett.* **56**, 919 (1986), [Erratum: *Phys. Rev. Lett.* **57**, 1192 (1986)].
 - [5] B. G. Eroziolmsky, I. A. Kuznetsov, I. A. Kujda, Y. A. Mostovoi, and I. V. Stepanenko, “New measurements of the electron - neutron spin asymmetry,” *Phys. Lett. B* **263**, 33–38 (1991), [Erratum: *Phys. Lett. B* **412**, 240 (1997)].
 - [6] P. Liaud, K. Schreckenbach, R. Kossakowski, H. Nastoll, A. Bussiere, J. P. Guillaud, and L. Beck, “The measurement of the beta asymmetry in the decay of polarized neutrons,” *Nucl. Phys. A* **612**, 53–81 (1997).
 - [7] Y. A. Mostovoi *et al.*, “Experimental value of G_A/G_V from a measurement of both P -odd correlations in free-neutron decay,” *Phys. Atom. Nucl.* **64**, 1955–1960 (2001).
 - [8] M. Schumann, M. Kreuz, M. Deissenroth, F. Glück, J. Krempel, B. Märkisch, D. Mund, A. Petoukhov, T. Soldner, and H. Abele, “Measurement of the Proton Asymmetry Parameter C in Neutron Beta Decay,” *Phys. Rev. Lett.* **100**, 151801 (2008), [arXiv:0712.2442 \[hep-ph\]](#).
 - [9] D. Mund, B. Märkisch, M. Deissenroth, J. Krempel, M. Schumann, H. Abele, A. Petoukhov, and T. Soldner, “Determination of the Weak Axial Vector Coupling $\lambda = g_A/g_V$ from a Measurement of the β -Asymmetry Parameter A in Neutron Beta Decay,” *Phys. Rev. Lett.* **110**, 172502 (2013), [arXiv:1204.0013 \[hep-ex\]](#).
 - [10] M. A. P. Brown *et al.* (UCNA), “New result for the neutron β -asymmetry parameter A_0 from UCNA,” *Phys. Rev. C* **97**, 035505 (2018), [arXiv:1712.00884 \[nucl-ex\]](#).
 - [11] B. Märkisch *et al.*, “Measurement of the Weak Axial-Vector Coupling Constant in the Decay of Free Neutrons Using a Pulsed Cold Neutron Beam,” *Phys. Rev. Lett.* **122**, 242501 (2019), [arXiv:1812.04666 \[nucl-ex\]](#).
 - [12] M. Beck *et al.*, “Improved determination of the β - $\bar{\nu}_e$

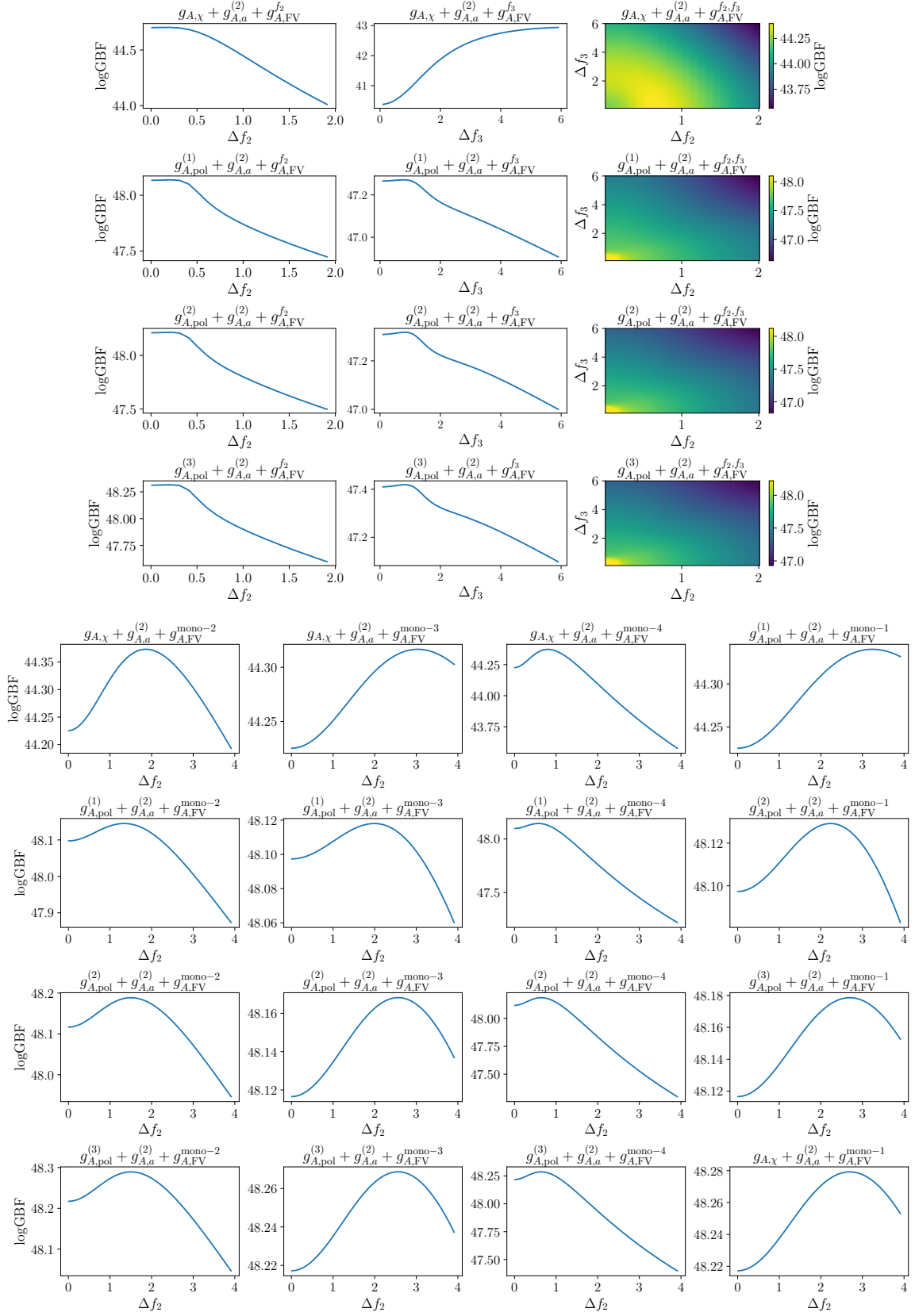


FIG. 8. The log of the Bayes factors obtained by fitting the data at all lattice spacings (keeping the largest volume ensemble for the pion masses for which multiple volumes are available) using the models of Eqs. (4.1) and Eq. (4.4a) plus the FV models of Eqs. (4.2) (upper) and Eqs. (4.3) (lower) that depend on f_2 or/and f_3 , the parameters whose prior width we vary.

TABLE III. The extrapolated g_A values of the 64 models included in the analysis along with the log Gaussian Bayes Factors representing the log-likelihood distribution, logGBF, and the normalized model weights, $P(M_k|D)$. Models are sorted by descending weight.

Model	Chiral	FV	Disc.	logGBF	$P(M_k D)$	$P(g_A M_k)$
poly3_F21_a2	(4.1d)	(4.3a)	(4.4a)	48.27	3.12×10^{-2}	1.2655(79)
poly3_F33_a2	(4.1d)	(4.3d)	(4.4a)	48.27	3.11×10^{-2}	1.2660(79)
poly3_F23_a2	(4.1d)	(4.3b)	(4.4a)	48.26	3.09×10^{-2}	1.2661(79)
poly3_F21_a4	(4.1d)	(4.3a)	(4.4b)	48.21	2.91×10^{-2}	1.2657(97)
poly3_F33_a4	(4.1d)	(4.3d)	(4.4b)	48.20	2.89×10^{-2}	1.2659(96)
poly3_F23_a4	(4.1d)	(4.3b)	(4.4b)	48.19	2.87×10^{-2}	1.2659(96)
poly2_F21_a2	(4.1c)	(4.3a)	(4.4a)	48.17	2.82×10^{-2}	1.2655(82)
poly2_F33_a2	(4.1c)	(4.3d)	(4.4a)	48.17	2.81×10^{-2}	1.2660(81)
poly2_F23_a2	(4.1c)	(4.3b)	(4.4a)	48.16	2.79×10^{-2}	1.2660(81)
poly1_F33_a2	(4.1b)	(4.3d)	(4.4a)	48.13	2.70×10^{-2}	1.2718(90)
poly1_F21_a2	(4.1b)	(4.3a)	(4.4a)	48.12	2.67×10^{-2}	1.2713(91)
poly1_F23_a2	(4.1b)	(4.3b)	(4.4a)	48.12	2.67×10^{-2}	1.2718(90)
poly2_F21_a4	(4.1c)	(4.3a)	(4.4b)	48.11	2.64×10^{-2}	1.2657(98)
poly2_F33_a4	(4.1c)	(4.3d)	(4.4b)	48.10	2.62×10^{-2}	1.2659(98)
poly2_F23_a4	(4.1c)	(4.3b)	(4.4b)	48.09	2.60×10^{-2}	1.2659(98)
poly1_F33_a4	(4.1b)	(4.3d)	(4.4b)	48.05	2.51×10^{-2}	1.271(11)
poly1_F21_a4	(4.1b)	(4.3a)	(4.4b)	48.05	2.49×10^{-2}	1.271(11)
poly1_F23_a4	(4.1b)	(4.3b)	(4.4b)	48.04	2.48×10^{-2}	1.271(11)
poly3_F31_a2	(4.1d)	(4.3c)	(4.4a)	47.93	2.22×10^{-2}	1.2651(79)
poly3_NNLOf2_a2	(4.1d)	(4.2b)	(4.4a)	47.90	2.15×10^{-2}	1.2654(81)
poly3_F31_a4	(4.1d)	(4.3c)	(4.4b)	47.87	2.09×10^{-2}	1.2655(97)
poly3_NNLOf2_a4	(4.1d)	(4.2b)	(4.4b)	47.84	2.01×10^{-2}	1.2658(97)
poly2_F31_a2	(4.1c)	(4.3c)	(4.4a)	47.83	2.01×10^{-2}	1.2650(82)
poly2_NNLOf2_a2	(4.1c)	(4.2b)	(4.4a)	47.80	1.95×10^{-2}	1.2654(83)
poly2_F31_a4	(4.1c)	(4.3c)	(4.4b)	47.77	1.90×10^{-2}	1.2655(98)
poly1_F31_a2	(4.1b)	(4.3c)	(4.4a)	47.76	1.87×10^{-2}	1.2707(91)
poly1_NNLOf2_a2	(4.1b)	(4.2b)	(4.4a)	47.74	1.83×10^{-2}	1.2710(92)
poly2_NNLOf2_a4	(4.1c)	(4.2b)	(4.4b)	47.74	1.82×10^{-2}	1.2657(99)
poly3_NNLO_a2	(4.1d)	(4.2a)	(4.4a)	47.73	1.80×10^{-2}	1.2656(80)
poly3_NNLOf2f3_a2	(4.1d)	(4.2d)	(4.4a)	47.71	1.78×10^{-2}	1.2649(80)
poly1_F31_a4	(4.1b)	(4.3c)	(4.4b)	47.69	1.75×10^{-2}	1.271(11)
poly1_NNLOf2_a4	(4.1b)	(4.2b)	(4.4b)	47.67	1.71×10^{-2}	1.271(11)
poly3_NNLO_a4	(4.1d)	(4.2a)	(4.4b)	47.66	1.68×10^{-2}	1.2654(97)
poly3_NNLOf2f3_a4	(4.1d)	(4.2d)	(4.4b)	47.65	1.67×10^{-2}	1.2654(97)
poly2_NNLO_a2	(4.1c)	(4.2a)	(4.4a)	47.62	1.63×10^{-2}	1.2656(82)
poly2_NNLOf2f3_a2	(4.1c)	(4.2d)	(4.4a)	47.61	1.61×10^{-2}	1.2648(83)
poly1_NNLOf2f3_a2	(4.1b)	(4.2d)	(4.4a)	47.56	1.54×10^{-2}	1.2704(92)
poly2_NNLO_a4	(4.1c)	(4.2a)	(4.4b)	47.56	1.52×10^{-2}	1.2654(98)
poly2_NNLOf2f3_a4	(4.1c)	(4.2d)	(4.4b)	47.55	1.51×10^{-2}	1.2654(99)
poly1_NNLO_a2	(4.1b)	(4.2a)	(4.4a)	47.55	1.51×10^{-2}	1.2713(91)
poly1_NNLOf2f3_a4	(4.1b)	(4.2d)	(4.4b)	47.50	1.43×10^{-2}	1.271(11)
poly1_NNLO_a4	(4.1b)	(4.2a)	(4.4b)	47.48	1.40×10^{-2}	1.271(11)
poly3_NNLOf3_a2	(4.1d)	(4.2c)	(4.4a)	47.42	1.32×10^{-2}	1.2662(79)
poly3_NNLOf3_a4	(4.1d)	(4.2c)	(4.4b)	47.35	1.23×10^{-2}	1.2658(97)
poly2_NNLOf3_a2	(4.1c)	(4.2c)	(4.4a)	47.32	1.20×10^{-2}	1.2661(82)
poly1_NNLOf3_a2	(4.1b)	(4.2c)	(4.4a)	47.27	1.14×10^{-2}	1.2720(91)
poly2_NNLOf3_a4	(4.1c)	(4.2c)	(4.4b)	47.25	1.12×10^{-2}	1.2658(98)
poly1_NNLOf3_a4	(4.1b)	(4.2c)	(4.4b)	47.20	1.07×10^{-2}	1.271(11)
chPT_NNLOf2_a2	(4.1a)	(4.2b)	(4.4a)	44.45	6.80×10^{-4}	1.266(10)
chPT_NNLOf2_a4	(4.1a)	(4.2b)	(4.4b)	44.39	6.41×10^{-4}	1.266(11)
chPT_F21_a2	(4.1a)	(4.3a)	(4.4a)	44.37	6.31×10^{-4}	1.267(11)
chPT_F21_a4	(4.1a)	(4.3a)	(4.4b)	44.31	5.93×10^{-4}	1.267(12)
chPT_F33_a2	(4.1a)	(4.3d)	(4.4a)	44.31	5.93×10^{-4}	1.268(11)
chPT_NNLOf2f3_a2	(4.1a)	(4.2d)	(4.4a)	44.30	5.88×10^{-4}	1.267(11)
chPT_F23_a2	(4.1a)	(4.3b)	(4.4a)	44.30	5.85×10^{-4}	1.268(11)
chPT_F33_a4	(4.1a)	(4.3d)	(4.4b)	44.25	5.59×10^{-4}	1.267(12)
chPT_NNLOf2f3_a4	(4.1a)	(4.2d)	(4.4b)	44.24	5.54×10^{-4}	1.267(12)
chPT_F23_a4	(4.1a)	(4.3b)	(4.4b)	44.24	5.52×10^{-4}	1.267(12)
chPT_F31_a2	(4.1a)	(4.3c)	(4.4a)	44.09	4.78×10^{-4}	1.266(11)
chPT_F31_a4	(4.1a)	(4.3c)	(4.4b)	44.03	4.50×10^{-4}	1.266(12)
chPT_NNLOf3_a2	(4.1a)	(4.2c)	(4.4a)	42.94	1.51×10^{-4}	1.267(10)
chPT_NNLOf3_a4	(4.1a)	(4.2c)	(4.4b)	42.91	1.46×10^{-4}	1.266(12)
chPT_NNLO_a4	(4.1a)	(4.2a)	(4.4b)	41.56	3.80×10^{-5}	1.267(12)
chPT_NNLO_a2	(4.1a)	(4.2a)	(4.4a)	41.51	3.61×10^{-5}	1.270(10)
Bayes Model Average						1.2674(96)

TABLE IV. Priors used in the model fits. The models are ordered according to the order in which the model Eqs. (4.1), (4.2), (4.3), and (4.5) appear in the main text.

Chiral FV	Disc.	g_0	\bar{c}_{34}	d_{16}^T	c_0	c_1	c_2	c_3	c_4	f_2	f_3	a_2	a_4	b_4	
(4.1a)	(4.2a)	(4.4a)	1.25(10)	0(1)	0(5)							0(0.5)			
		(4.4b)	1.25(10)	0(1)	0(5)							0(0.5)	0(0.25)	0(0.5)	
	(4.2b)	(4.4a)	1.25(10)	0(1)	0(5)					0(1)		0(0.5)			
		(4.4b)	1.25(10)	0(1)	0(5)					0(1)		0(0.5)	0(0.25)	0(0.5)	
	(4.2c)	(4.4a)	1.25(10)	0(1)	0(5)						0(6)	0(0.5)			
		(4.4b)	1.25(10)	0(1)	0(5)						0(6)	0(0.5)	0(0.25)	0(0.5)	
	(4.2d)	(4.4a)	1.25(10)	0(1)	0(5)					0(1)	0(6)	0(0.5)			
		(4.4b)	1.25(10)	0(1)	0(5)					0(1)	0(6)	0(0.5)	0(0.25)	0(0.5)	
	(4.3a)	(4.4a)	1.25(10)	0(1)	0(5)					0(2)		0(0.5)			
		(4.4b)	1.25(10)	0(1)	0(5)					0(2)		0(0.5)	0(0.25)	0(0.5)	
	(4.3b)	(4.4a)	1.25(10)	0(1)	0(5)					0(2)		0(0.5)			
		(4.4b)	1.25(10)	0(1)	0(5)					0(2)		0(0.5)	0(0.25)	0(0.5)	
	(4.3c)	(4.4a)	1.25(10)	0(1)	0(5)					0(2)		0(0.5)			
		(4.4b)	1.25(10)	0(1)	0(5)					0(2)		0(0.5)	0(0.25)	0(0.5)	
	(4.3d)	(4.4a)	1.25(10)	0(1)	0(5)					0(2)		0(0.5)			
		(4.4b)	1.25(10)	0(1)	0(5)					0(2)		0(0.5)	0(0.25)	0(0.5)	
(4.1b)	(4.2a)	(4.4a)	1.25(50)	0(1)		1.25(10)	0(0.5)	0(0.5)				0(0.5)			
		(4.4b)	1.25(50)	0(1)		1.25(10)	0(0.5)	0(0.5)				0(0.5)	0(0.25)	0(0.5)	
	(4.2b)	(4.4a)	1.25(50)	0(1)		1.25(10)	0(0.5)	0(0.5)		0(1)		0(0.5)			
		(4.4b)	1.25(50)	0(1)		1.25(10)	0(0.5)	0(0.5)		0(1)		0(0.5)	0(0.25)	0(0.5)	
	(4.2c)	(4.4a)	1.25(50)	0(1)		1.25(10)	0(0.5)	0(0.5)			0(1)	0(0.5)			
		(4.4b)	1.25(50)	0(1)		1.25(10)	0(0.5)	0(0.5)			0(1)	0(0.5)	0(0.25)	0(0.5)	
	(4.2d)	(4.4a)	1.25(50)	0(1)		1.25(10)	0(0.5)	0(0.5)		0(1)	0(1)	0(0.5)			
		(4.4b)	1.25(50)	0(1)		1.25(10)	0(0.5)	0(0.5)		0(1)	0(1)	0(0.5)	0(0.25)	0(0.5)	
	(4.3a)	(4.4a)				1.25(10)	0(0.5)	0(0.5)		0(2)		0(0.5)			
		(4.4b)				1.25(10)	0(0.5)	0(0.5)		0(2)		0(0.5)	0(0.25)	0(0.5)	
	(4.3b)	(4.4a)				1.25(10)	0(0.5)	0(0.5)		0(2)		0(0.5)			
		(4.4b)				1.25(10)	0(0.5)	0(0.5)		0(2)		0(0.5)	0(0.25)	0(0.5)	
	(4.3c)	(4.4a)				1.25(10)	0(0.5)	0(0.5)		0(2)		0(0.5)			
		(4.4b)				1.25(10)	0(0.5)	0(0.5)		0(2)		0(0.5)	0(0.25)	0(0.5)	
	(4.3d)	(4.4a)				1.25(10)	0(0.5)	0(0.5)		0(2)		0(0.5)			
		(4.4b)				1.25(10)	0(0.5)	0(0.5)		0(2)		0(0.5)	0(0.25)	0(0.5)	
(4.1c)	(4.2a)	(4.4a)	1.25(50)	0(1)		1.25(10)		0(1)	0(1)			0(0.5)			
		(4.4b)	1.25(50)	0(1)		1.25(10)		0(1)	0(1)			0(0.5)	0(0.25)	0(0.5)	
	(4.2b)	(4.4a)	1.25(50)	0(1)		1.25(10)		0(1)	0(1)	0(1)		0(0.5)			
		(4.4b)	1.25(50)	0(1)		1.25(10)		0(1)	0(1)	0(1)		0(0.5)	0(0.25)	0(0.5)	
	(4.2c)	(4.4a)	1.25(50)	0(1)		1.25(10)		0(1)	0(1)		0(1)	0(0.5)			
		(4.4b)	1.25(50)	0(1)		1.25(10)		0(1)	0(1)		0(1)	0(0.5)	0(0.25)	0(0.5)	
	(4.2d)	(4.4a)	1.25(50)	0(1)		1.25(10)		0(1)	0(1)	0(1)	0(1)	0(0.5)			
		(4.4b)	1.25(50)	0(1)		1.25(10)		0(1)	0(1)	0(1)	0(1)	0(0.5)	0(0.25)	0(0.5)	
	(4.3a)	(4.4a)				1.25(10)		0(1)	0(1)		0(2)		0(0.5)		
		(4.4b)				1.25(10)		0(1)	0(1)		0(2)		0(0.5)	0(0.25)	0(0.5)
	(4.3b)	(4.4a)				1.25(10)		0(1)	0(1)		0(2)		0(0.5)		
		(4.4b)				1.25(10)		0(1)	0(1)		0(2)		0(0.5)	0(0.25)	0(0.5)
	(4.3c)	(4.4a)				1.25(10)		0(1)	0(1)		0(2)		0(0.5)		
		(4.4b)				1.25(10)		0(1)	0(1)		0(2)		0(0.5)	0(0.25)	0(0.5)
	(4.3d)	(4.4a)				1.25(10)		0(1)	0(1)		0(2)		0(0.5)		
		(4.4b)				1.25(10)		0(1)	0(1)		0(2)		0(0.5)	0(0.25)	0(0.5)
(4.1d)	(4.2a)	(4.4a)	1.25(50)	0(1)		1.25(10)		0(1)		0(1)		0(0.5)			
		(4.4b)	1.25(50)	0(1)		1.25(10)		0(1)		0(1)		0(0.5)	0(0.25)	0(0.5)	
	(4.2b)	(4.4a)	1.25(50)	0(1)		1.25(10)		0(1)		0(1)	0(1)	0(0.5)			
		(4.4b)	1.25(50)	0(1)		1.25(10)		0(1)		0(1)	0(1)	0(0.5)	0(0.25)	0(0.5)	
	(4.2c)	(4.4a)	1.25(50)	0(1)		1.25(10)		0(1)		0(1)		0(1)	0(0.5)		
		(4.4b)	1.25(50)	0(1)		1.25(10)		0(1)		0(1)	0(1)	0(0.5)	0(0.25)	0(0.5)	
	(4.2d)	(4.4a)	1.25(50)	0(1)		1.25(10)		0(1)		0(1)	0(1)	0(0.5)			
		(4.4b)	1.25(50)	0(1)		1.25(10)		0(1)		0(1)	0(1)	0(0.5)	0(0.25)	0(0.5)	
	(4.3a)	(4.4a)				1.25(10)		0(1)		0(1)	0(2)		0(0.5)		
		(4.4b)				1.25(10)		0(1)		0(1)	0(2)		0(0.5)	0(0.25)	0(0.5)
	(4.3b)	(4.4a)				1.25(10)		0(1)		0(1)	0(2)		0(0.5)		
		(4.4b)				1.25(10)		0(1)		0(1)	0(2)		0(0.5)	0(0.25)	0(0.5)
	(4.3c)	(4.4a)				1.25(10)		0(1)		0(1)	0(2)		0(0.5)		
		(4.4b)				1.25(10)		0(1)		0(1)	0(2)		0(0.5)	0(0.25)	0(0.5)
	(4.3d)	(4.4a)				1.25(10)		0(1)		0(1)	0(2)		0(0.5)		
		(4.4b)				1.25(10)		0(1)		0(1)	0(2)		0(0.5)	0(0.25)	0(0.5)

angular correlation coefficient a in free neutron decay with the a SPECT spectrometer,” *Phys. Rev. C* **101**, 055506 (2020), arXiv:1908.04785 [nucl-ex].

- [13] M. T. Hassan *et al.*, “Measurement of the neutron decay electron-antineutrino angular correlation by the aCORN experiment,” *Phys. Rev. C* **103**, 045502 (2021), arXiv:2012.14379 [nucl-ex].
- [14] S. Navas *et al.* (Particle Data Group), “Review of par-

title physics,” *Phys. Rev. D* **110**, 030001 (2024).

- [15] R. Kossakowski, P. Liaud, G. Azuelos, P. Grivot, and K. Schreckenbach, “Neutron Lifetime Measurement With a Helium Filled Time Projection Chamber,” *Nucl. Phys. A* **503**, 473–500 (1989).
- [16] J. Byrne and P. G. Dawber, “A Revised Value for the Neutron Lifetime Measured Using a Penning Trap,” *EPL* **33**, 187 (1996).

TABLE V. Posterior values of the parameters from each model fit. The models are ordered according to the order in which the model Eqs. (4.1), (4.2), (4.3), and (4.5) appear in the main text.

Chiral FV	Disc.	g_0	\tilde{c}_{34}	d_{16}^T	c_0	c_1	c_2	c_3	c_4	f_2	f_3	a_2	a_4	b_4	
(4.1a)	(4.2a)	(4.4a)	1.226(15)	0.81(24)	-4.95(33)							-0.025(50)	-0.08(24)	-1.5(1.7)	
	(4.2b)	(4.4a)	1.212(20)	0.80(24)	-4.77(37)							0.10(14)	0.008(244)	-0.5(1.7)	
	(4.2c)	(4.4a)	1.223(15)	0.79(25)	-4.92(33)							0.033(54)	0.008(244)	-0.5(1.7)	
	(4.2d)	(4.4b)	1.212(21)	0.77(25)	-4.76(39)							0.022(54)	0.008(244)	-0.4(1.7)	
	(4.3a)	(4.4a)	1.222(15)	0.76(24)	-4.87(33)							0.11(14)	0.008(244)	-0.4(1.7)	
	(4.3b)	(4.4a)	1.221(16)	0.77(24)	-4.86(34)							0.030(54)	0.008(244)	-0.4(1.7)	
	(4.3c)	(4.4a)	1.222(15)	0.77(24)	-4.87(33)							0.06(14)	0.008(244)	-0.4(1.7)	
	(4.3d)	(4.4a)	1.222(16)	0.77(24)	-4.86(34)							0.022(53)	0.008(244)	-0.4(1.7)	
	(4.2a)	(4.4a)	0.79(38)	0.50(95)	1.302(22)	-0.24(17)	-0.20(38)					0.028(89)	0.009(52)	-0.009(243)	-0.04(48)
	(4.2b)	(4.4a)	1.27(46)	0.30(95)	1.296(31)	-0.24(17)	-0.17(39)					0.028(89)	0.04(14)	0.007(243)	-0.4(1.7)
	(4.2c)	(4.4a)	0.75(39)	0.23(99)	1.297(31)	-0.22(18)	-0.19(40)					0.41(97)	0.04(14)	0.01(24)	-0.3(1.7)
	(4.2d)	(4.4b)	1.37(44)	-0.04(1.00)	1.303(22)	-0.24(17)	-0.18(38)					0.40(97)	0.003(51)	-0.01(24)	-0.5(1.7)
(4.3a)	(4.4a)	1.302(23)	-0.24(17)	-0.19(39)	1.302(22)	-0.24(17)	-0.18(40)				-0.40(59)	0.03(14)	0.02(24)	-0.1(1.7)	
(4.3b)	(4.4a)	1.303(22)	-0.24(17)	-0.19(38)	1.302(23)	-0.24(17)	-0.19(39)				-1.2(1.4)	0.016(51)	0.001(242)	-0.03(48)	
(4.3c)	(4.4a)	1.301(22)	-0.24(17)	-0.19(38)	1.302(23)	-0.24(17)	-0.19(39)				1.0(1.7)	0.007(50)	-0.01(24)	-0.03(48)	
(4.3d)	(4.4a)	1.301(23)	-0.24(17)	-0.19(39)	1.301(22)	-0.24(17)	-0.19(38)				1.0(1.7)	0.013(88)	-0.01(24)	-0.03(48)	
(4.2a)	(4.4a)	0.79(38)	0.52(95)	1.275(10)	-0.24(17)	-0.18(39)					0.023(89)	0.023(89)	0.02(24)	-0.02(48)	
(4.2b)	(4.4a)	1.29(46)	0.32(96)	1.275(10)	-0.24(17)	-0.19(38)					-1.0(1.7)	0.007(50)	0.02(24)	-0.02(48)	
(4.2c)	(4.4a)	0.76(39)	0.26(99)	1.275(10)	-0.24(17)	-0.19(38)					0.46(97)	0.013(51)	-0.01(24)	-0.03(48)	
(4.2d)	(4.4b)	1.38(44)	-0.03(1.00)	1.275(10)	-0.24(17)	-0.19(38)					0.44(97)	0.05(14)	0.004(242)	-0.5(1.7)	
(4.3a)	(4.4a)	1.276(12)	-0.75(33)	1.276(12)	-0.75(32)	0.08(88)					-0.41(58)	0.038(54)	0.04(24)	-0.2(1.7)	
(4.3b)	(4.4a)	1.276(10)	-0.76(32)	1.276(10)	-0.76(32)	0.08(88)					-0.41(59)	0.04(14)	0.04(24)	-0.2(1.7)	
(4.3c)	(4.4a)	1.275(10)	-0.75(32)	1.275(10)	-0.75(32)	0.08(88)					-1.3(1.4)	0.027(51)	0.02(24)	-0.03(48)	
(4.3d)	(4.4a)	1.276(10)	-0.76(32)	1.276(10)	-0.76(32)	0.08(88)					-1.3(1.4)	0.023(88)	0.006(241)	-0.04(48)	
(4.2a)	(4.4a)	0.79(38)	0.52(95)	1.2758(91)	-0.75(15)	-0.68(88)					0.13(96)	0.019(52)	0.007(241)	-0.04(48)	
(4.2b)	(4.4a)	1.29(46)	0.32(96)	1.272(18)	-0.68(28)	-0.75(15)					0.14(97)	0.05(14)	0.01(24)	-0.5(1.7)	
(4.2c)	(4.4a)	0.75(39)	0.27(99)	1.275(18)	-0.75(15)	-0.75(15)					0.13(96)	0.035(53)	0.03(24)	-0.3(1.7)	
(4.2d)	(4.4b)	1.38(44)	-0.02(1.00)	1.276(18)	-0.75(15)	-0.75(15)					0.46(97)	0.013(51)	0.004(242)	-0.5(1.7)	
(4.3a)	(4.4a)	1.275(10)	-0.75(32)	1.274(18)	-0.71(28)	-0.74(15)					-0.41(58)	0.038(53)	0.04(24)	-0.2(1.7)	
(4.3b)	(4.4a)	1.275(10)	-0.75(32)	1.274(18)	-0.71(28)	-0.74(15)					-0.09(98)	0.04(14)	0.02(24)	-0.03(48)	
(4.3c)	(4.4a)	1.275(10)	-0.75(32)	1.275(10)	-0.75(32)	-0.75(16)					0.15(96)	0.018(88)	0.006(241)	-0.04(48)	
(4.3d)	(4.4a)	1.276(10)	-0.76(32)	1.276(10)	-0.76(32)	-0.75(15)					-0.09(98)	0.027(51)	0.02(24)	-0.03(48)	
(4.2a)	(4.4a)	0.80(38)	0.51(95)	1.2758(91)	-0.75(15)	-0.68(88)					0.13(96)	0.019(51)	0.007(241)	-0.04(48)	
(4.2b)	(4.4a)	1.29(46)	0.32(96)	1.275(18)	-0.75(15)	-0.75(15)					0.14(96)	0.05(14)	0.01(24)	-0.5(1.7)	
(4.2c)	(4.4a)	0.75(39)	0.27(99)	1.276(18)	-0.75(15)	-0.75(15)					0.13(97)	0.035(53)	0.03(24)	-0.3(1.7)	
(4.2d)	(4.4b)	1.38(44)	-0.03(1.00)	1.274(18)	-0.71(28)	-0.74(15)					0.14(96)	0.013(51)	0.004(242)	-0.5(1.7)	
(4.3a)	(4.4a)	1.275(10)	-0.75(32)	1.274(18)	-0.71(28)	-0.74(15)					-0.41(58)	0.038(53)	0.04(24)	-0.2(1.7)	
(4.3b)	(4.4a)	1.275(10)	-0.75(32)	1.274(18)	-0.71(28)	-0.74(15)					-0.09(98)	0.04(14)	0.02(24)	-0.03(48)	
(4.3c)	(4.4a)	1.275(10)	-0.75(32)	1.275(10)	-0.75(32)	-0.75(16)					0.15(96)	0.018(88)	0.006(241)	-0.04(48)	
(4.3d)	(4.4a)	1.276(10)	-0.76(32)	1.276(10)	-0.76(32)	-0.75(15)					-0.09(98)	0.027(51)	0.02(24)	-0.03(48)	

- [17] J. S. Nico *et al.*, “Measurement of the neutron lifetime by counting trapped protons in a cold neutron beam,” *Phys. Rev. C* **71**, 055502 (2005), [arXiv:nucl-ex/0411041](#).
- [18] A. T. Yue, M. S. Dewey, D. M. Gilliam, G. L. Greene, A. B. Laptev, J. S. Nico, W. M. Snow, and F. E. Wietfeldt, “Improved Determination of the Neutron Lifetime,” *Phys. Rev. Lett.* **111**, 222501 (2013), [arXiv:1309.2623 \[nucl-ex\]](#).
- [19] A. Serebrov *et al.*, “Measurement of the neutron lifetime using a gravitational trap and a low-temperature Fomblin coating,” *Phys. Lett. B* **605**, 72–78 (2005), [arXiv:nucl-ex/0408009](#).
- [20] A. Pichlmaier, V. Varlamov, K. Schreckenbach, and P. Geltenbort, “Neutron lifetime measurement with the UCN trap-in-trap MAMBO II,” *Phys. Lett. B* **693**, 221–226 (2010).
- [21] A. Steyerl, J. M. Pendlebury, C. Kaufman, S. S. Malik, and A. M. Desai, “Quasielastic scattering in the interaction of ultracold neutrons with a liquid wall and application in a reanalysis of the Mambo I neutron-lifetime experiment,” *Phys. Rev. C* **85**, 065503 (2012).
- [22] S. Arzumanov, L. Bondarenko, S. Chernyavsky, P. Geltenbort, V. Morozov, V. V. Nesvizhevsky, Y. Panin, and A. Strepetov, “A measurement of the neutron lifetime using the method of storage of ultracold neutrons and detection of inelastically up-scattered neutrons,” *Phys. Lett. B* **745**, 79–89 (2015).
- [23] A. P. Serebrov *et al.*, “Neutron lifetime measurements with a large gravitational trap for ultracold neutrons,” *Phys. Rev. C* **97**, 055503 (2018), [arXiv:1712.05663 \[nucl-ex\]](#).
- [24] R. W. Pattie, Jr. *et al.*, “Measurement of the neutron lifetime using a magneto-gravitational trap and in situ detection,” *Science* **360**, 627–632 (2018), [arXiv:1707.01817 \[nucl-ex\]](#).
- [25] V. F. Ezhov *et al.*, “Measurement of the neutron lifetime with ultra-cold neutrons stored in a magneto-gravitational trap,” *JETP Lett.* **107**, 671–675 (2018), [arXiv:1412.7434 \[nucl-ex\]](#).
- [26] F. M. Gonzalez *et al.* (UCN τ), “Improved neutron lifetime measurement with UCN τ ,” *Phys. Rev. Lett.* **127**, 162501 (2021), [arXiv:2106.10375 \[nucl-ex\]](#).
- [27] R. Musedinovic *et al.*, “Measurement of the Free Neutron Lifetime in a Magneto-Gravitational Trap with In Situ Detection,” (2024), [arXiv:2409.05560 \[nucl-ex\]](#).
- [28] B. Fornal and B. Grinstein, “Dark Matter Interpretation of the Neutron Decay Anomaly,” *Phys. Rev. Lett.* **120**, 191801 (2018), [Erratum: *Phys. Rev. Lett.* **124**, 219901 (2020)], [arXiv:1801.01124 \[hep-ph\]](#).
- [29] Y. Fuwa *et al.*, “Improved measurements of neutron lifetime with cold neutron beam at J-PARC,” (2024), [arXiv:2412.19519 \[nucl-ex\]](#).
- [30] A. Czarnecki, W. J. Marciano, and A. Sirlin, “Neutron Lifetime and Axial Coupling Connection,” *Phys. Rev. Lett.* **120**, 202002 (2018), [arXiv:1802.01804 \[hep-ph\]](#).
- [31] V. Cirigliano, W. Dekens, E. Mereghetti, and O. Tomalak, “Effective field theory for radiative corrections to charged-current processes: Vector coupling,” *Phys. Rev. D* **108**, 053003 (2023), [arXiv:2306.03138 \[hep-ph\]](#).
- [32] P. Vander Griend, Z. Cao, R. Hill, and R. Plestid, “The Fermi function and the neutron’s lifetime,” (2025), [arXiv:2501.17916 \[hep-ph\]](#).
- [33] A. Sirlin, “General Properties of the Electromagnetic Corrections to the Beta Decay of a Physical Nucleon,” *Phys. Rev.* **164**, 1767–1775 (1967).
- [34] A. Sirlin, “Current Algebra Formulation of Radiative Corrections in Gauge Theories and the Universality of the Weak Interactions,” *Rev. Mod. Phys.* **50**, 573 (1978), [Erratum: *Rev. Mod. Phys.* **50**, 905 (1978)].
- [35] C.-Y. Seng, M. Gorchtein, H. H. Patel, and M. J. Ramsey-Musolf, “Reduced Hadronic Uncertainty in the Determination of V_{ud} ,” *Phys. Rev. Lett.* **121**, 241804 (2018), [arXiv:1807.10197 \[hep-ph\]](#).
- [36] C. Y. Seng, M. Gorchtein, and M. J. Ramsey-Musolf, “Dispersive evaluation of the inner radiative correction in neutron and nuclear β decay,” *Phys. Rev. D* **100**, 013001 (2019), [arXiv:1812.03352 \[nucl-th\]](#).
- [37] A. Czarnecki, W. J. Marciano, and A. Sirlin, “Radiative Corrections to Neutron and Nuclear Beta Decays Revisited,” *Phys. Rev. D* **100**, 073008 (2019), [arXiv:1907.06737 \[hep-ph\]](#).
- [38] L. Hayen, “Standard model $\mathcal{O}(\alpha)$ renormalization of g_A and its impact on new physics searches,” *Phys. Rev. D* **103**, 113001 (2021), [arXiv:2010.07262 \[hep-ph\]](#).
- [39] L. Hayen, “Radiative corrections to nucleon weak charges and Beyond Standard Model impact,” (2021), [arXiv:2102.03458 \[hep-ph\]](#).
- [40] M. Gorchtein and C.-Y. Seng, “The Standard Model Theory of Neutron Beta Decay,” *Universe* **9**, 422 (2023), [arXiv:2307.01145 \[hep-ph\]](#).
- [41] V. Cirigliano, J. de Vries, L. Hayen, E. Mereghetti, and A. Walker-Loud, “Pion-Induced Radiative Corrections to Neutron β Decay,” *Phys. Rev. Lett.* **129**, 121801 (2022), [arXiv:2202.10439 \[nucl-th\]](#).
- [42] E. E. Jenkins and A. V. Manohar, “Baryon chiral perturbation theory using a heavy fermion Lagrangian,” *Phys. Lett. B* **255**, 558–562 (1991).
- [43] E. E. Jenkins and A. V. Manohar, “Chiral corrections to the baryon axial currents,” *Phys. Lett. B* **259**, 353–358 (1991).
- [44] T. Bhattacharya, V. Cirigliano, S. Cohen, R. Gupta, H.-W. Lin, and B. Yoon, “Axial, Scalar and Tensor Charges of the Nucleon from 2+1+1-flavor Lattice QCD,” *Phys. Rev. D* **94**, 054508 (2016), [arXiv:1606.07049 \[hep-lat\]](#).
- [45] C. C. Chang, A. Nicholson, E. Rinaldi, E. Berkowitz, N. Garron, D. A. Brantley, H. Monge-Camacho, C. J. Monahan, C. Bouchard, M. A. Clark, B. Joó, T. Kurth, K. Orginos, P. Vranas, and A. Walker-Loud, “A percent-level determination of the nucleon axial coupling from quantum chromodynamics,” *Nature* **558**, 91–94 (2018), [arXiv:1805.12130 \[hep-lat\]](#).
- [46] R. Gupta, Y.-C. Jang, B. Yoon, H.-W. Lin, V. Cirigliano, and T. Bhattacharya, “Isovector Charges of the Nucleon from 2+1+1-flavor Lattice QCD,” *Phys. Rev. D* **98**, 034503 (2018), [arXiv:1806.09006 \[hep-lat\]](#).
- [47] C. Alexandrou, S. Bacchio, M. Constantinou, J. Finkenrath, K. Hadjiyiannakou, K. Jansen, G. Koutsou, and A. Vaquero Aviles-Casco, “Nucleon axial, tensor, and scalar charges and σ -terms in lattice QCD,” *Phys. Rev. D* **102**, 054517 (2020), [arXiv:1909.00485 \[hep-lat\]](#).
- [48] G. S. Bali, S. Collins, S. Heybrock, M. Löffler, R. Rödl, W. Söldner, and S. Weishäupl (RQCD), “Octet baryon isovector charges from $N_f = 2 + 1$ lattice QCD,” *Phys. Rev. D* **108**, 034512 (2023), [arXiv:2305.04717 \[hep-lat\]](#).
- [49] D. Djukanovic, G. von Hippel, H. B. Meyer, K. Ottnad, and H. Wittig, “Improved analysis of isovector nucleon matrix elements with $N_f = 2 + 1$ flavors of $\mathcal{O}(a)$

- improved Wilson fermions,” *Phys. Rev. D* **109**, 074507 (2024), [arXiv:2402.03024 \[hep-lat\]](#).
- [50] C. Alexandrou, S. Bacchio, J. Finkenrath, C. Iona, G. Koutsou, Y. Li, and G. Spanoudes, “Nucleon charges and σ -terms in lattice QCD,” (2024), [arXiv:2412.01535 \[hep-lat\]](#).
- [51] C.-Y. Seng, “Hybrid analysis of radiative corrections to neutron decay with current algebra and effective field theory,” *JHEP* **07**, 175 (2024), [arXiv:2403.08976 \[hep-ph\]](#).
- [52] V. Cirigliano, W. Dekens, E. Mereghetti, and O. Tomalak, “Effective field theory for radiative corrections to charged-current processes II: Axial-vector coupling,” (2024), [arXiv:2410.21404 \[nucl-th\]](#).
- [53] V. Cirigliano, A. Crivellin, M. Hoferichter, and M. Moulson, “Scrutinizing CKM unitarity with a new measurement of the $K_{\mu 3}/K_{\mu 2}$ branching fraction,” *Phys. Lett. B* **838**, 137748 (2023), [arXiv:2208.11707 \[hep-ph\]](#).
- [54] J. C. Hardy and I. S. Towner, “Superallowed $0^+ \rightarrow 0^+$ nuclear β decays: 2020 critical survey, with implications for V_{ud} and CKM unitarity,” *Phys. Rev. C* **102**, 045501 (2020).
- [55] V. Cirigliano, W. Dekens, J. de Vries, S. Gandolfi, M. Hoferichter, and E. Mereghetti, “Radiative Corrections to Superallowed β Decays in Effective Field Theory,” *Phys. Rev. Lett.* **133**, 211801 (2024), [arXiv:2405.18469 \[hep-ph\]](#).
- [56] V. Cirigliano, W. Dekens, J. de Vries, S. Gandolfi, M. Hoferichter, and E. Mereghetti, “Ab initio electroweak corrections to superallowed β decays and their impact on V_{ud} ,” *Phys. Rev. C* **110**, 055502 (2024), [arXiv:2405.18464 \[nucl-th\]](#).
- [57] S. Alioli, V. Cirigliano, W. Dekens, J. de Vries, and E. Mereghetti, “Right-handed charged currents in the era of the Large Hadron Collider,” *JHEP* **05**, 086 (2017), [arXiv:1703.04751 \[hep-ph\]](#).
- [58] V. Cirigliano, W. Dekens, J. de Vries, E. Mereghetti, and T. Tong, “Anomalies in global SMEFT analyses. A case study of first-row CKM unitarity,” *JHEP* **03**, 033 (2024), [arXiv:2311.00021 \[hep-ph\]](#).
- [59] V. Cirigliano, D. Díaz-Calderón, A. Falkowski, M. González-Alonso, and A. Rodríguez-Sánchez, “Semileptonic tau decays beyond the Standard Model,” *JHEP* **04**, 152 (2022), [arXiv:2112.02087 \[hep-ph\]](#).
- [60] R. G. Edwards, G. T. Fleming, P. Hägler, J. W. Negele, K. Orginos, A. V. Pochinsky, D. B. Renner, D. G. Richards, and W. Schroers (LHPC), “The Nucleon axial charge in full lattice QCD,” *Phys. Rev. Lett.* **96**, 052001 (2006), [arXiv:hep-lat/0510062 \[hep-lat\]](#).
- [61] C. Drischler, W. Haxton, K. McElvain, E. Mereghetti, A. Nicholson, P. Vranas, and A. Walker-Loud, “Towards grounding nuclear physics in QCD,” *Prog. Part. Nucl. Phys.* **121**, 103888 (2021), [arXiv:1910.07961 \[nucl-th\]](#).
- [62] J. Gasser and H. Leutwyler, “Spontaneously Broken Symmetries: Effective Lagrangians at Finite Volume,” *Nucl. Phys. B* **307**, 763–778 (1988).
- [63] R. L. Jaffe, “Delocalization of the axial charge in the chiral limit,” *Phys. Lett. B* **529**, 105–110 (2002), [arXiv:hep-ph/0108015 \[hep-ph\]](#).
- [64] T. D. Cohen, “The Extraction of g_A from finite volume systems: The Long and short of it,” *Phys. Lett. B* **529**, 50–56 (2002), [arXiv:hep-lat/0112014 \[hep-lat\]](#).
- [65] T. Yamazaki, Y. Aoki, T. Blum, H. W. Lin, M. F. Lin, S. Ohta, S. Sasaki, R. J. Tweedie, and J. M. Zanotti (RBC+UKQCD), “Nucleon axial charge in 2+1 flavor dynamical lattice QCD with domain wall fermions,” *Phys. Rev. Lett.* **100**, 171602 (2008), [arXiv:0801.4016 \[hep-lat\]](#).
- [66] T. Yamazaki, Y. Aoki, T. Blum, H.-W. Lin, S. Ohta, S. Sasaki, R. Tweedie, and J. Zanotti, “Nucleon form factors with 2+1 flavor dynamical domain-wall fermions,” *Phys. Rev. D* **79**, 114505 (2009), [arXiv:0904.2039 \[hep-lat\]](#).
- [67] S. Capitani, M. Della Morte, G. von Hippel, B. Jager, A. Jüttner, B. Knippschild, H. B. Meyer, and H. Wittig, “The nucleon axial charge from lattice QCD with controlled errors,” *Phys. Rev. D* **86**, 074502 (2012), [arXiv:1205.0180 \[hep-lat\]](#).
- [68] A. Walker-Loud *et al.*, “Lattice QCD Determination of g_A ,” *PoS CD2018*, 020 (2020), [arXiv:1912.08321 \[hep-lat\]](#).
- [69] S. R. Beane and M. J. Savage, “Baryon axial charge in a finite volume,” *Phys. Rev. D* **70**, 074029 (2004), [arXiv:hep-ph/0404131 \[hep-ph\]](#).
- [70] A. Walker-Loud *et al.*, “Light hadron spectroscopy using domain wall valence quarks on an Asqtad sea,” *Phys. Rev. D* **79**, 054502 (2009), [arXiv:0806.4549 \[hep-lat\]](#).
- [71] E. E. Jenkins, “Chiral Lagrangian for baryons in the $1/N_c$ expansion,” *Phys. Rev. D* **53**, 2625–2644 (1996), [arXiv:hep-ph/9509433 \[hep-ph\]](#).
- [72] T. R. Hemmert, B. R. Holstein, and J. Kambor, “ $\Delta(1232)$ and the polarizabilities of the nucleon,” *Phys. Rev. D* **55**, 5598–5612 (1997), [arXiv:hep-ph/9612374](#).
- [73] R. Flores-Mendieta, C. P. Hofmann, E. E. Jenkins, and A. V. Manohar, “On the structure of large N_c cancellations in baryon chiral perturbation theory,” *Phys. Rev. D* **62**, 034001 (2000), [arXiv:hep-ph/0001218](#).
- [74] E. E. Jenkins, X.-d. Ji, and A. V. Manohar, “ $\Delta \rightarrow N\gamma$ in large- N_c QCD,” *Phys. Rev. Lett.* **89**, 242001 (2002), [arXiv:hep-ph/0207092](#).
- [75] D. Siemens, J. Ruiz de Elvira, E. Epelbaum, M. Hoferichter, H. Krebs, B. Kubis, and U.-G. Meißner, “Reconciling threshold and subthreshold expansions for pion-nucleon scattering,” *Phys. Lett. B* **770**, 27–34 (2017), [arXiv:1610.08978 \[nucl-th\]](#).
- [76] T. R. Hemmert, B. R. Holstein, and J. Kambor, “Chiral Lagrangians and $\Delta(1232)$ interactions: Formalism,” *J. Phys. G* **24**, 1831–1859 (1998), [arXiv:hep-ph/9712496](#).
- [77] R. F. Dashen and A. V. Manohar, “Baryon - pion couplings from large- N_c QCD,” *Phys. Lett. B* **315**, 425–430 (1993), [arXiv:hep-ph/9307241](#).
- [78] R. F. Dashen and A. V. Manohar, “ $1/N_c$ corrections to the baryon axial currents in QCD,” *Phys. Lett. B* **315**, 438–440 (1993), [arXiv:hep-ph/9307242 \[hep-ph\]](#).
- [79] A. Calle Cordon and J. L. Goity, “Baryon Masses and Axial Couplings in the Combined $1/N_c$ and Chiral Expansions,” *Phys. Rev. D* **87**, 016019 (2013), [arXiv:1210.2364 \[nucl-th\]](#).
- [80] T. R. Hemmert, M. Procura, and W. Weise, “Quark mass dependence of the nucleon axial vector coupling constant,” *Phys. Rev. D* **68**, 075009 (2003), [arXiv:hep-lat/0303002 \[hep-lat\]](#).
- [81] J. Kambor and M. Mojžiš, “Field redefinitions and wave function renormalization to $\mathcal{O}(p^4)$ in heavy baryon chiral perturbation theory,” *JHEP* **04**, 031 (1999), [arXiv:hep-ph/9901235 \[hep-ph\]](#).

- [82] T. Becher and H. Leutwyler, “Low energy analysis of $\pi N \rightarrow \pi N$,” *JHEP* **06**, 017 (2001), [arXiv:hep-ph/0103263](#).
- [83] J. Gasser, M. A. Ivanov, E. Lipartia, M. Mojžiš, and A. Rusetsky, “Ground state energy of pionic hydrogen to one loop,” *Eur. Phys. J. C* **26**, 13–34 (2002), [arXiv:hep-ph/0206068](#).
- [84] R. F. Dashen, E. E. Jenkins, and A. V. Manohar, “The $1/N_c$ expansion for baryons,” *Phys. Rev. D* **49**, 4713 (1994), [Erratum: *Phys. Rev. D* **51**, 2489 (1995)], [arXiv:hep-ph/9310379](#).
- [85] R. F. Dashen, E. E. Jenkins, and A. V. Manohar, “Spin flavor structure of large- N_c baryons,” *Phys. Rev. D* **51**, 3697–3727 (1995), [arXiv:hep-ph/9411234](#).
- [86] G. Karl and J. E. Paton, “Naive Quark Model for an Arbitrary Number of Colors,” *Phys. Rev. D* **30**, 238 (1984).
- [87] E. E. Jenkins, “Large- N_c baryons,” *Ann. Rev. Nucl. Part. Sci.* **48**, 81–119 (1998), [arXiv:hep-ph/9803349](#).
- [88] R. Flores-Mendieta and C. P. Hofmann, “Renormalization of the baryon axial vector current in large- N_c chiral perturbation theory,” *Phys. Rev. D* **74**, 094001 (2006), [arXiv:hep-ph/0609120](#).
- [89] R. Flores-Mendieta, M. A. Hernandez-Ruiz, and C. P. Hofmann, “Renormalization of the baryon axial vector current in large- N_c chiral perturbation theory: Effects of the decuplet-octet mass difference and flavor symmetry breaking,” *Phys. Rev. D* **86**, 094041 (2012), [arXiv:1210.8445 \[hep-ph\]](#).
- [90] R. Flores-Mendieta, C. I. Garcia, and J. Hernandez, “Baryon axial vector current in large- N_c chiral perturbation theory: Complete analysis for $N_c = 3$,” *Phys. Rev. D* **103**, 094032 (2021), [arXiv:2102.06100 \[hep-ph\]](#).
- [91] R. Flores-Mendieta and G. Sanchez-Almanza, “Universality of the baryon axial vector current operator in large- N_c chiral perturbation theory,” (2024), [arXiv:2411.19838 \[hep-ph\]](#).
- [92] J. Bulava, A. D. Hanlon, B. Hörz, C. Morningstar, A. Nicholson, F. Romero-López, S. Skinner, P. Vranas, and A. Walker-Loud, “Elastic nucleon-pion scattering at $m_\pi=200$ MeV from lattice QCD,” *Nucl. Phys. B* **987**, 116105 (2023), [arXiv:2208.03867 \[hep-lat\]](#).
- [93] L. Barca, G. Bali, and S. Collins, “Toward N to $N\pi$ matrix elements from lattice QCD,” *Phys. Rev. D* **107**, L051505 (2023), [arXiv:2211.12278 \[hep-lat\]](#).
- [94] V. Bernard and U.-G. Meißner, “The Nucleon axial-vector coupling beyond one loop,” *Phys. Lett. B* **639**, 278–282 (2006), [arXiv:hep-lat/0605010 \[hep-lat\]](#).
- [95] N. Miller *et al.*, “Scale setting the Möbius domain wall fermion on gradient-flowed HISQ action using the omega baryon mass and the gradient-flow scales t_0 and w_0 ,” *Phys. Rev. D* **103**, 054511 (2021), [arXiv:2011.12166 \[hep-lat\]](#).
- [96] D. B. Renner, W. Schroers, R. Edwards, G. T. Fleming, P. Hagler, J. W. Negele, K. Orginos, A. V. Pochinski, and D. Richards (LHP), “Hadronic physics with domain-wall valence and improved staggered sea quarks,” *Nucl. Phys. B Proc. Suppl.* **140**, 255–260 (2005), [arXiv:hep-lat/0409130](#).
- [97] O. Bär, G. Rupak, and N. Shoresh, “Simulations with different lattice Dirac operators for valence and sea quarks,” *Phys. Rev. D* **67**, 114505 (2003), [arXiv:hep-lat/0210050 \[hep-lat\]](#).
- [98] E. Follana, Q. Mason, C. Davies, K. Hornbostel, G. P. Lepage, J. Shigemitsu, H. Trottier, and K. Wong (HPQCD, UKQCD), “Highly improved staggered quarks on the lattice, with applications to charm physics,” *Phys. Rev. D* **75**, 054502 (2007), [arXiv:hep-lat/0610092 \[hep-lat\]](#).
- [99] R. C. Brower, H. Neff, and K. Orginos, “Möbius fermions: Improved domain wall chiral fermions,” *Nucl. Phys. B Proc. Suppl.* **140**, 686–688 (2005), [arXiv:hep-lat/0409118](#).
- [100] R. C. Brower, H. Neff, and K. Orginos, “Möbius fermions,” *Nucl. Phys. B Proc. Suppl.* **153**, 191–198 (2006), [arXiv:hep-lat/0511031](#).
- [101] M. Lüscher, “Properties and uses of the Wilson flow in lattice QCD,” *JHEP* **1008**, 071 (2010), [arXiv:1006.4518 \[hep-lat\]](#).
- [102] R. Lohmayer and H. Neuberger, “Continuous smearing of Wilson Loops,” *PoS LATTICE2011*, 249 (2011), [arXiv:1110.3522 \[hep-lat\]](#).
- [103] E. Berkowitz, C. Bouchard, C. Chang, M. Clark, B. Joo, T. Kurth, C. Monahan, A. Nicholson, K. Orginos, E. Rinaldi, P. Vranas, and A. Walker-Loud, “Möbius Domain-Wall fermions on gradient-flowed dynamical HISQ ensembles,” *Phys. Rev. D* **96**, 054513 (2017), [arXiv:1701.07559 \[hep-lat\]](#).
- [104] A. Bazavov *et al.* (MILC), “Scaling studies of QCD with the dynamical HISQ action,” *Phys. Rev. D* **82**, 074501 (2010), [arXiv:1004.0342 \[hep-lat\]](#).
- [105] A. Bazavov *et al.* (MILC), “Lattice QCD ensembles with four flavors of highly improved staggered quarks,” *Phys. Rev. D* **87**, 054505 (2013), [arXiv:1212.4768 \[hep-lat\]](#).
- [106] N. Miller *et al.*, “ F_K/F_π from Möbius Domain-Wall fermions solved on gradient-flowed HISQ ensembles,” *Phys. Rev. D* **102**, 034507 (2020), [arXiv:2005.04795 \[hep-lat\]](#).
- [107] M. A. Clark, R. Babich, K. Barros, R. C. Brower, and C. Rebbi (QUADA), “Solving Lattice QCD systems of equations using mixed precision solvers on GPUs,” *Comput. Phys. Commun.* **181**, 1517–1528 (2010), [arXiv:0911.3191 \[hep-lat\]](#).
- [108] R. Babich, M. Clark, B. Joo, G. Shi, R. Brower, *et al.*, “Scaling Lattice QCD beyond 100 GPUs,” (2011), [arXiv:1109.2935 \[hep-lat\]](#).
- [109] S. Borsányi, S. Dürr, Z. Fodor, C. Hoelbling, S. D. Katz, S. Krieg, T. Kurth, L. Lellouch, T. Lippert, and C. McNeile (BMW), “High-precision scale setting in lattice QCD,” *JHEP* **09**, 010 (2012), [arXiv:1203.4469 \[hep-lat\]](#).
- [110] T. Bhattacharya, V. Cirigliano, S. Cohen, R. Gupta, A. Joseph, H.-W. Lin, and B. Yoon (PNDME), “Iso-vector and Iso-scalar Tensor Charges of the Nucleon from Lattice QCD,” *Phys. Rev. D* **92**, 094511 (2015), [arXiv:1506.06411 \[hep-lat\]](#).
- [111] C. Bouchard, C. C. Chang, T. Kurth, K. Orginos, and A. Walker-Loud, “On the Feynman-Hellmann Theorem in Quantum Field Theory and the Calculation of Matrix Elements,” *Phys. Rev. D* **96**, 014504 (2017), [arXiv:1612.06963 \[hep-lat\]](#).
- [112] K. Symanzik, “Continuum Limit and Improved Action in Lattice Theories. 2. $O(N)$ Nonlinear Sigma Model in Perturbation Theory,” *Nucl. Phys. B* **226**, 205–227 (1983).
- [113] K. Symanzik, “Continuum Limit and Improved Action in Lattice Theories. 1. Principles and ϕ^4 Theory,” *Nucl. Phys. B* **226**, 187–204 (1983).
- [114] O. Bär, C. Bernard, G. Rupak, and N. Shoresh, “Chi-

- ral perturbation theory for staggered sea quarks and Ginsparg-Wilson valence quarks,” *Phys. Rev. D* **72**, 054502 (2005), [arXiv:hep-lat/0503009 \[hep-lat\]](#).
- [115] Y. Aoki *et al.* (Flavour Lattice Averaging Group (FLAG)), “FLAG Review 2024,” (2024), [arXiv:2411.04268 \[hep-lat\]](#).
- [116] E. Berkowitz, C. Bouchard, D. B. Brantley, C. Chang, M. Clark, N. Garron, B. Joó, T. Kurth, C. Monahan, H. Monge-Camacho, A. Nicholson, K. Orginos, E. Rinaldi, P. Vranas, and A. Walker-Loud, “An accurate calculation of the nucleon axial charge with lattice QCD,” (2017), [arXiv:1704.01114 \[hep-lat\]](#).
- [117] N. Yamanaka, S. Hashimoto, T. Kaneko, and H. Ohki (JLQCD), “Nucleon charges with dynamical overlap fermions,” *Phys. Rev. D* **98**, 054516 (2018), [arXiv:1805.10507 \[hep-lat\]](#).
- [118] J. Liang, Y.-B. Yang, T. Draper, M. Gong, and K.-F. Liu, “Quark spins and Anomalous Ward Identity,” *Phys. Rev. D* **98**, 074505 (2018), [arXiv:1806.08366 \[hep-ph\]](#).
- [119] K.-I. Ishikawa, Y. Kuramashi, S. Sasaki, N. Tsukamoto, A. Ukawa, and T. Yamazaki (PACS), “Nucleon form factors on a large volume lattice near the physical point in 2+1 flavor QCD,” *Phys. Rev. D* **98**, 074510 (2018), [arXiv:1807.03974 \[hep-lat\]](#).
- [120] E. Shintani, K.-I. Ishikawa, Y. Kuramashi, S. Sasaki, and T. Yamazaki, “Nucleon form factors and root-mean-square radii on a $(10.8 \text{ fm})^4$ lattice at the physical point,” *Phys. Rev. D* **99**, 014510 (2019), [Erratum: *Phys. Rev. D* **102**, 019902 (2020)], [arXiv:1811.07292 \[hep-lat\]](#).
- [121] T. Harris, G. von Hippel, P. Junnarkar, H. B. Meyer, K. Ottnad, J. Wilhelm, H. Wittig, and L. Wrang, “Nucleon isovector charges and twist-2 matrix elements with $N_f = 2 + 1$ dynamical Wilson quarks,” *Phys. Rev. D* **100**, 034513 (2019), [arXiv:1905.01291 \[hep-lat\]](#).
- [122] N. Hasan, J. Green, S. Meinel, M. Engelhardt, S. Krieg, J. Negele, A. Pochinsky, and S. Syritsyn, “Nucleon axial, scalar, and tensor charges using lattice QCD at the physical pion mass,” *Phys. Rev. D* **99**, 114505 (2019), [arXiv:1903.06487 \[hep-lat\]](#).
- [123] G. S. Bali, L. Barca, S. Collins, M. Gruber, M. Löffler, A. Schäfer, W. Söldner, P. Wein, S. Weishäupl, and T. Wurm (RQCD), “Nucleon axial structure from lattice QCD,” *JHEP* **05**, 126 (2020), [arXiv:1911.13150 \[hep-lat\]](#).
- [124] S. Park, R. Gupta, B. Yoon, S. Mondal, T. Bhattacharya, Y.-C. Jang, B. Joó, and F. Winter (Nucleon Matrix Elements (NME)), “Precision nucleon charges and form factors using $(2+1)$ -flavor lattice QCD,” *Phys. Rev. D* **105**, 054505 (2022), [arXiv:2103.05599 \[hep-lat\]](#).
- [125] D. Djukanovic, G. von Hippel, J. Koponen, H. B. Meyer, K. Ottnad, T. Schulz, and H. Wittig, “Isovector axial form factor of the nucleon from lattice QCD,” *Phys. Rev. D* **106**, 074503 (2022), [arXiv:2207.03440 \[hep-lat\]](#).
- [126] R. Tsuji, N. Tsukamoto, Y. Aoki, K.-I. Ishikawa, Y. Kuramashi, S. Sasaki, E. Shintani, and T. Yamazaki (PACS), “Nucleon isovector couplings in $N_f = 2 + 1$ lattice QCD at the physical point,” *Phys. Rev. D* **106**, 094505 (2022), [arXiv:2207.11914 \[hep-lat\]](#).
- [127] C. Alexandrou, S. Bacchio, M. Constantinou, J. Finkenrath, R. Frezzotti, B. Kostrzewa, G. Koutsou, G. Spanoudes, and C. Urbach (Extended Twisted Mass), “Nucleon axial and pseudoscalar form factors using twisted-mass fermion ensembles at the physical point,” *Phys. Rev. D* **109**, 034503 (2024), [arXiv:2309.05774 \[hep-lat\]](#).
- [128] R. E. Smail *et al.* (QCDSF/UKQCD/CSSM), “Constraining beyond the standard model nucleon isovector charges,” *Phys. Rev. D* **108**, 094511 (2023), [arXiv:2304.02866 \[hep-lat\]](#).
- [129] R. Tsuji, Y. Aoki, K.-I. Ishikawa, Y. Kuramashi, S. Sasaki, K. Sato, E. Shintani, H. Watanabe, and T. Yamazaki (PACS), “Nucleon form factors in $N_f = 2 + 1$ lattice QCD at the physical point: Finite lattice spacing effect on the root-mean-square radii,” *Phys. Rev. D* **109**, 094505 (2024), [arXiv:2311.10345 \[hep-lat\]](#).
- [130] Y.-C. Jang, R. Gupta, T. Bhattacharya, B. Yoon, and H.-W. Lin (Precision Neutron Decay Matrix Elements (PNDME)), “Nucleon isovector axial form factors,” *Phys. Rev. D* **109**, 014503 (2024), [arXiv:2305.11330 \[hep-lat\]](#).
- [131] E. Epelbaum, H. Krebs, and P. Reinert, “High-precision nuclear forces from chiral EFT: State-of-the-art, challenges and outlook,” *Front. in Phys.* **8**, 98 (2020), [arXiv:1911.11875 \[nucl-th\]](#).
- [132] M. Hoferichter, J. Ruiz de Elvira, B. Kubis, and U.-G. Meißner, “Matching pion–nucleon Roy–Steiner equations to chiral perturbation theory,” *Phys. Rev. Lett.* **115**, 192301 (2015), [arXiv:1507.07552 \[nucl-th\]](#).
- [133] M. Hoferichter, J. Ruiz de Elvira, B. Kubis, and U.-G. Meißner, “Roy–Steiner-equation analysis of pion–nucleon scattering,” *Phys. Rept.* **625**, 1–88 (2016), [arXiv:1510.06039 \[hep-ph\]](#).
- [134] K. Hebel, “Three-nucleon forces: Implementation and applications to atomic nuclei and dense matter,” *Phys. Rept.* **890**, 1–116 (2021), [arXiv:2002.09548 \[nucl-th\]](#).
- [135] H. Krebs, “Nuclear Currents in Chiral Effective Field Theory,” *Eur. Phys. J. A* **56**, 234 (2020), [arXiv:2008.00974 \[nucl-th\]](#).
- [136] I. Tews *et al.*, “Nuclear Forces for Precision Nuclear Physics: A Collection of Perspectives,” *Few Body Syst.* **63**, 67 (2022), [arXiv:2202.01105 \[nucl-th\]](#).
- [137] M. Hoferichter, J. Menéndez, and A. Schwenk, “Coherent elastic neutrino–nucleus scattering: EFT analysis and nuclear responses,” *Phys. Rev. D* **102**, 074018 (2020), [arXiv:2007.08529 \[hep-ph\]](#).
- [138] A. Manohar and H. Georgi, “Chiral Quarks and the Nonrelativistic Quark Model,” *Nucl. Phys. B* **234**, 189–212 (1984).
- [139] M. Hoferichter, E. Mereghetti, J. Ruiz de Elvira, D. Siemans, and A. Walker-Loud, In preparation.
- [140] “LALIBÉ: CalLat Collaboration code for lattice qcd calculations,” <https://github.com/callat-qcd/lalibe>.
- [141] R. G. Edwards and B. Joo (SciDAC, LHPC, UKQCD), “The Chroma software system for lattice QCD,” *Nucl. Phys. B Proc. Suppl.* **140**, 832 (2005), [arXiv:hep-lat/0409003](#).
- [142] The HDF Group, “Hierarchical Data Format, version 5,” (1997-NNNN), <http://www.hdfgroup.org/HDF5/>.
- [143] T. Kurth, A. Pochinsky, A. Sarje, S. Syritsyn, and A. Walker-Loud, “High-Performance I/O: HDF5 for Lattice QCD,” *PoS LATTICE2014*, 045 (2015), [arXiv:1501.06992 \[hep-lat\]](#).
- [144] E. Berkowitz, “METAQ: Bundle Supercomputing Tasks,” (2017), <https://github.com/evanberkowitz/metaq>, [arXiv:1702.06122 \[physics.comp-ph\]](#).
- [145] E. Berkowitz, G. R. Jansen, K. McElvain, and

- A. Walker-Loud, “Job Management and Task Bundling,” *EPJ Web Conf.* **175**, 09007 (2018), [arXiv:1710.01986 \[hep-lat\]](https://arxiv.org/abs/1710.01986).
- [146] “MILC Collaboration code for lattice qcd calculations,” https://github.com/milc-qcd/milc_qcd.
- [147] P. Lepage, “gplepage/gvar,” (2020), <https://github.com/gplepage/gvar>.
- [148] P. Lepage, “gplepage/lqfit,” (2020), <https://github.com/gplepage/lqfit>.
- [149] R. Gupta, S. Park, M. Hoferichter, E. Mereghetti, B. Yoon, and T. Bhattacharya, “Pion–Nucleon Sigma Term from Lattice QCD,” *Phys. Rev. Lett.* **127**, 242002 (2021), [arXiv:2105.12095 \[hep-lat\]](https://arxiv.org/abs/2105.12095).
- [150] R. Gupta, T. Bhattacharya, M. Hoferichter, E. Mereghetti, S. Park, and B. Yoon, “The pion–nucleon sigma term from Lattice QCD,” *PoS CD2021*, 060 (2024), [arXiv:2203.13862 \[hep-lat\]](https://arxiv.org/abs/2203.13862).
- [151] D. Siemens, “Elastic pion–nucleon scattering in chiral perturbation theory: Explicit $\Delta(1232)$ degrees of freedom,” (2020), [arXiv:2001.03906 \[nucl-th\]](https://arxiv.org/abs/2001.03906).